

Dissertation

zur Erlangung des Doktorgrades der Fakultät für Chemie und Pharmazie
der Ludwig-Maximilians-Universität München



**Identification of microRNAs regulating adipocyte
differentiation *via* mTOR nutrient-signaling**

Theresa Christina Käuferle

aus Aichach

2015

Dissertation zur Erlangung des Doktorgrades
der Fakultät für Chemie und Pharmazie
der Ludwig-Maximilians-Universität München

**Identification of microRNAs regulating adipocyte
differentiation *via* mTOR nutrient-signaling**

Theresa Christina Käuferle

aus

Aichach, Deutschland

2015

Erklärung

Diese Dissertation wurde im Sinne von § 7 der Promotionsordnung vom 28. November 2011 von Herrn Prof. Dr. Adelbert Roscher betreut und von Herrn Prof. Dr. Klaus Förstemann vor der Fakultät für Chemie und Pharmazie vertreten.

Eidesstattliche Versicherung

Diese Dissertation wurde eigenständig und ohne unerlaubte Hilfe erarbeitet.

München, den 07.04.2015

.....
(Unterschrift des Autors)

Dissertation eingereicht am:	10.04.2015
1. Gutachter:	Herr Prof. Dr. Klaus Förstemann
2. Gutachter:	Herr Prof. Dr. Adelbert Roscher
Mündliche Prüfung am:	06.05.2015

Meinen Eltern

„I'm still confused, but on a higher level“

(Enrico Fermi)

Inhalt

A	Introduction	1
1.	Adipocyte differentiation in obesity.....	1
2.	Adipocyte differentiation.....	1
2.1	Sequential gene expression during adipocyte differentiation.....	1
2.2	Stimulatory regulators of adipocyte differentiation.....	2
3.	mTOR nutrient signaling	3
3.1	Upstream regulators of mTOR.....	4
3.2	Cellular processes downstream of mTOR.....	5
3.3	mTOR inhibition by rapamycin	6
4.	miRNAs in gene regulation	7
4.1	Biology of miRNAs.....	7
4.2	MiRNA biogenesis and mechanism of action	7
4.3	MiRNAs in adipogenesis and nutrient sensing	9
5.	Aims of the thesis.....	10
B	Material and Methods.....	11
1.	Material.....	11
1.1	Sources of chemicals, reagents and enzymes	11
1.2	Buffers and solutions	12
1.3	Plasmids and oligonucleotides.....	14
1.4	Antibodies.....	15
1.5	Commercial kits	16
1.6	Cell lines	16
1.7	Consumables.....	16
1.8	Equipment and software	17
2.	Methods.....	18
2.1	<i>In silico</i> target prediction	18
2.2	Luciferase reporter assay	18
2.3	Transfection experiment	21
2.4	Differentiation experiment.....	21
2.5	RNA/DNA analysis.....	23
2.6	Immunoblot analysis	25
2.7	Flow cytometry analysis.....	25
2.8	Statistical analysis	26

C	Results	27
1.	3T3-L1 adipocyte model characterization.....	27
2.	<i>In silico</i> target prediction	28
3.	Functional validation of miRNA-target gene pairs	30
4.	MiRNA-mediated regulation of mTOR effectors	33
5.	MiRNA-mediated effects on adipocyte differentiation	35
6.	Candidate targets for miRNA effects upstream Tsc1.....	40
7.	Evaluation of miRNA families and clusters on adipocyte differentiation.....	41
D	Discussion.....	45
1.	Rapamycin alters expression of miRNAs	45
2.	Selected miRNAs target predicted genes.....	46
2.1	<i>In silico</i> target prediction	46
2.2	Functional confirmation by luciferase-based reporter assays	47
2.3	Functional confirmation by transfection experiments.....	48
2.4	Functional confirmation on protein level	49
3.	Effects of selected miRNAs on mTOR-signaling	51
4.	Effects of selected miRNAs on adipocyte differentiation	52
5.	MiRNA cluster 183/96/182 and miRNA family 103/107	56
E	Summary.....	58
F	References.....	59
G	Appendix	66
1.	Supplementary data.....	66
2.	List of abbreviations	73
3.	Curriculum vitae and publications	75
4.	Acknowledgements.....	76

A Introduction

1. Adipocyte differentiation in obesity

Obesity is defined as abnormal or excessive fat accumulation which may have adverse effects on health¹. According to World Health organization, people with a Body Mass Index (BMI) of 30 or more are obese (BMI = body weight in kilograms divided by the square of body height in metres: kg/m²). More than 2.8 million adults die each year from obesity-related diseases such as metabolic syndrome, type 2 diabetes, musculo-skeletal disorders and cardiovascular diseases¹. The increasing prevalence of obesity is not only a growing public health problem, but also a policy challenge as its consequences have been responsible for 2-8 % of public health service costs².

In the pathogenetic chain of events leading to obesity and its systemic complications multiple mechanisms of food intake control become important³. Fuel-communicating hormones as well as circulating nutrients can be detected by neurons resulting in control of food intake, energy expenditure and glucose homeostasis. On adipose tissue level the development of obesity involves adipocyte hypertrophy (increase in fat cell size), adipogenesis (increase in fat cell number) and angiogenesis (formation of blood vessels)⁴. Adipogenesis is mainly stimulated in times of caloric intake exceeding nutritional requirements and includes pre-adipocyte proliferation as well as adipocyte differentiation.

2. Adipocyte differentiation

2.1 Sequential gene expression during adipocyte differentiation

Whereas pre-adipocyte proliferation implies the replication of adipocyte precursors, adipocyte differentiation includes the transition from fibroblast-like, stellate-shaped precursor cells into mature, spherical adipocytes accumulating lipid droplets⁴. The changes in cell shape are accompanied by molecular changes, such as alterations in gene expression patterns resulting in an increased ability for lipid synthesis⁴⁻⁶ (**Figure 1**).

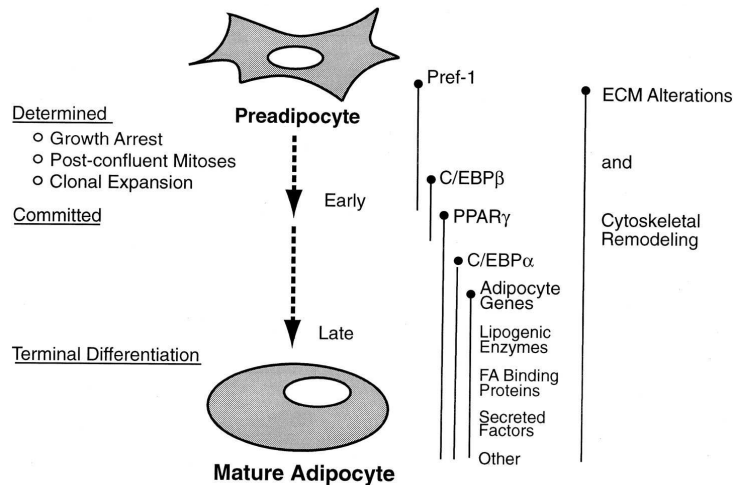


Figure 1: Overview of stages in adipocyte differentiation

Taken from Gregoire *et al.*⁵.

Before differentiation the cells undergo growth arrest as well as at least one round of cell doubling. The early stage of differentiation is associated with the disappearance of pre-adipocyte marker delta-like 1 homolog Dlk1 (*alias* pre-adipocyte factor Pref-1). Although the mechanism of Dlk1-mediated adipocyte differentiation inhibition remains to be elucidated, Dlk1 may possibly function by interacting with extracellular matrix proteins or acting as ligand for a pre-adipocyte receptor. Resulting morphological changes from fibroblastic to spherical cell shape are paralleled by changes in extracellular matrix and cytoskeletal components. ‘CCAAT/enhancer binding protein’ C/ebp β expression increases transiently resulting in ‘peroxisome proliferator-activated receptor’ Ppar γ expression stimulation. Subsequently C/ebp α is induced whereas the expression of C/ebp β declines again and Ppar γ expression is maintained. During terminal differentiation C/ebp α and Ppar γ transactivate the expression of adipocyte-specific genes involved in glucose and lipid metabolism to engage lipogenesis. Moreover insulin receptor abundance and thus insulin sensitivity increases and the cell begins to synthesize adipocyte-secreted products such as leptin thereby representing a highly specialized endocrine cell.

2.2 Stimulatory regulators of adipocyte differentiation

Much of what is known about regulation of adipocyte differentiation comes from 3T3-L1 adipocytes, a cell line which has been developed in the 1970s by Green and Kehinde from Swiss 3T3 mouse embryos⁷. 3T3-L1 cells can either stay in pre-adipocyte stadium or differentiate after stimulation and the mechanisms for adipogenic conversion as well

as their morphological and biochemical characteristics of 3T3-L1 cells have been described as similar to those of normal adipocytes *in vivo*. Moreover these cells have several practical advantages over primary preadipocytes^{4, 5}. Firstly, they provide a continuous source of cells as they differentiate with high efficiency also after high passage numbers, whereas primary adipocytes require a constant fresh supply due to their limited lifetime in cell culture. Secondly, 3T3-L1 cells are a homogenous population, all in the same stage of differentiation and thirdly they can be used for the study of both, early and late adipogenic events. An advantage of primary preadipocytes is that they can be isolated from adipose tissue of various species, at different postnatal stages of development and from various anatomic locations^{4, 5}.

In vitro studies have uncovered the mechanisms that drive the adipogenic process, involving extracellular signals such as nutrient sufficiency, cAMP elevating agents, hormonal and paracrine regulators⁴⁻⁶. 3T3-L1 cells for example can differentiate into mature adipocytes in high-glucose growth medium after stimulation with a combination of agents including 'isobutyl-methylxanthine' IBMX, dexamethasone and insulin⁴. Isobutyl-methylxanthine IBMX enhances adipocyte differentiation by increasing intracellular cAMP levels resulting in increased C/ebp β expression. Just like hormones in general, insulin and dexamethasone also mediate adipogenic effects by inducing transcription of adipogenic genes *via* specific receptors. Insulin stimulates Ppar γ expression *via* Igf-I receptor activation whereas the synthetic glucocorticoid dexamethasone up-regulates C/ebp δ *via* glucocorticoid receptor activation. The most essential paracrine signaling molecule 'insulin-like growth factor' Igf-I is secreted by expanding adipocytes and shares its mechanism with insulin. Further, nutrient sufficiency, such as high glucose levels induces adipocyte differentiation by increasing C/ebp α and Ppar γ levels.

3. mTOR nutrient signaling

Various nutrient-signaling pathways are responsible for adapting cell differentiation as well as cell growth to nutrient availability towards maintenance of whole-body metabolic homeostasis⁸. Among these, the mechanistic target of rapamycin (mTOR) pathway is an evolutionary conserved and well-studied intracellular nutrient-signaling pathway involved in the regulation of adipocyte differentiation, lipogenesis and intracellular accumulation of triglycerides^{8, 9}. mTOR itself is a multifunctional protein kinase consisting of two distinct complexes, termed mTOR complex 1 (mTORC1) and mTOR complex 2 (mTORC2) differing in their protein composition. mTORC1 consists of the

catalytic subunit mTOR, the positive mTOR regulator G β L and 'regulatory associated protein of mTOR complex 1' Rptor, which is involved in substrate recognition. mTORC2 includes mTOR, G β L and 'Rptor independent companion of mTOR complex 2' (Rictor). By integrating sufficiency of nutrients, energy and oxygen as well as signals from growth factors and hormones, the mTOR pathway regulates various cellular processes affecting cell growth and differentiation (**Figure 2**).

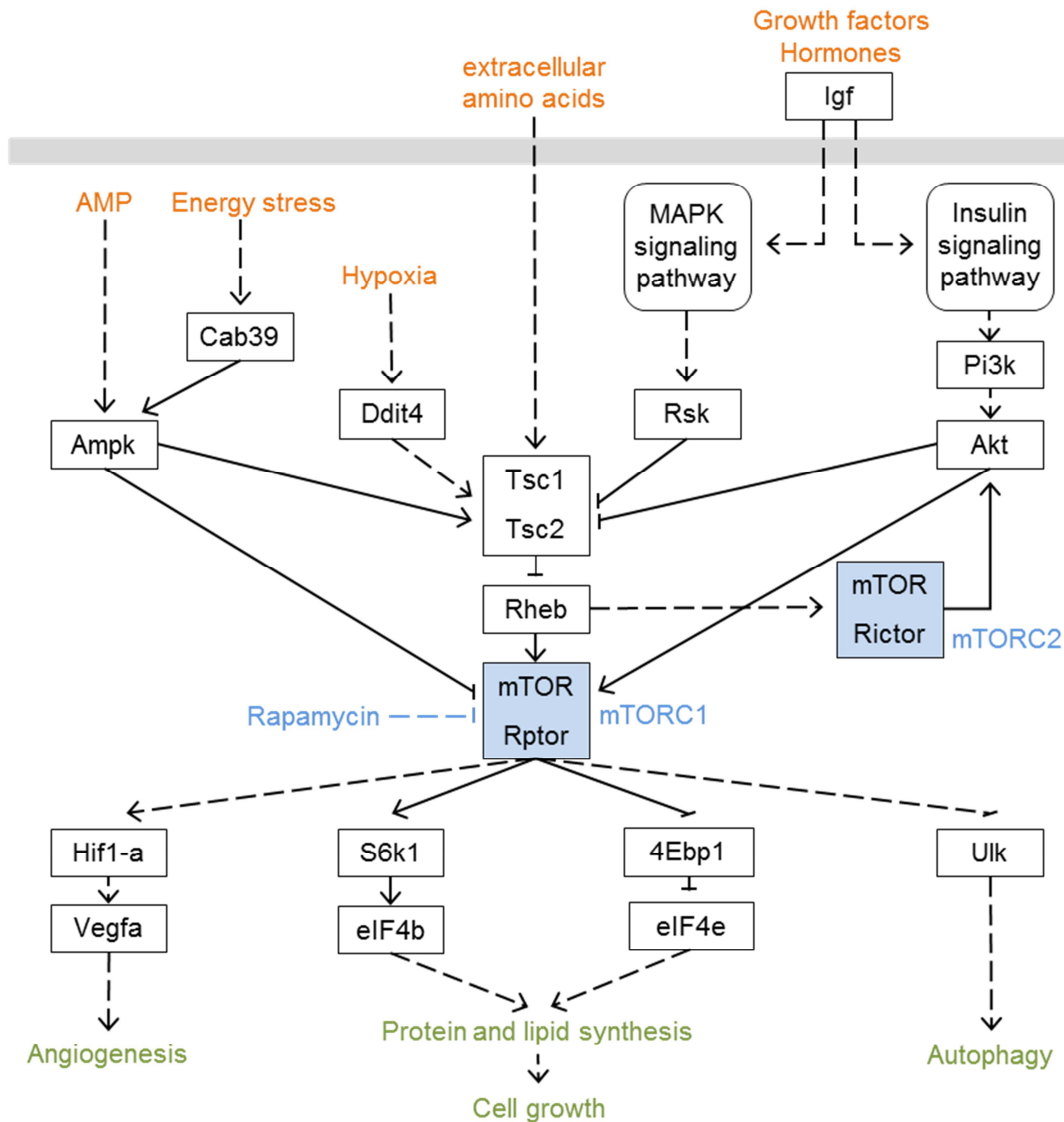


Figure 2: Simplified scheme of mTOR pathway

3.1 Upstream regulators of mTOR

In mammals both TOR complexes are controlled by growth factors and hormones whereas only mTORC1 responds to nutrients, energy stress and hypoxia¹⁰⁻¹². Insulin

and Igf bind to their receptors, which in turn activate key transduction pathways such as the insulin or the MAPK signaling pathway. In case of activated insulin signaling 'phosphatidylinositol 3-kinase' Pi3k is stimulated leading to phosphorylation of 'thymoma viral proto-oncogene' Akt. MAPK signaling cascade in the end stimulates 'ribosomal protein S6 kinase' Rsk. Both cascades result in mTORC1 stimulation *via* 'tuberous sclerosis complex' (Tsc) inhibition. Tsc includes Tsc1 (*alias* hamartin) and Tsc2 (*alias* tuberin) forming a physical and functional complex which acts *via* Rheb as an important negative regulator of mTORC1. However, Akt can also promote mTORC1 activity in a Tsc-independent manner. mTORC2 responds to growth factors through a Pi3k-dependent mechanism, which is poorly defined.

Nutrients, energy stress and hypoxia control mTOR signaling only *via* mTORC1. Firstly it has long been known that re-addition of amino acids, such as leucine, to starved cells can strongly stimulate mTORC1 activity, but the mechanism behind is not yet fully understood. Secondly, since cell growth is an energy-intensive process, mTOR nutrient signaling is also regulated by an energy sensor. Ampk is activated by increased intracellular AMP or ADP levels that can occur during energy stress. Ampk activation can also be triggered by Cab39, which in turn is also activated under conditions of energy stress. Ampk then blocks mTORC1 signaling *via* Tsc2 or Rptor. Thirdly, cellular metabolism is dependent on sufficient oxygen. Hypoxia inhibits mTORC1 by inducing Ddit4 expression, which in turn activates mTORC1 inhibitor Tsc.

3.2 Cellular processes downstream of mTOR

mTOR senses these upstream signals in order to control various components of the translation machinery, angiogenesis and regulation of autophagy¹⁰⁻¹². Protein synthesis is adapted to nutrient availability through translation initiation of a subset of genes *via* phosphorylation of S6k1 and 4Ebp1. mTORC1-mediated S6k1 phosphorylation of Thr389 results in phosphorylation of translation initiation factors and RNA binding proteins such as eIF4b thereby driving efficient translation. mTORC1-mediated 4Ebp1 phosphorylation prevents its inhibitory activity by leading to dissociation from eIF4e thereby allowing initiation of translation. *Via* a widely unknown mechanism, mTORC1 activates the translation of many lipogenic genes such as fatty acid synthase.

Experiments especially in the cancer field of mTOR-research show that tissue growth beyond a certain size is dependent on angiogenesis and that mTOR serves as a central regulator¹³. Stimulated by hypoxia, mTORC1 increases 'vascular endothelial growth factor' (Vegfa) gene expression *via* Hif1- α ¹⁴.

Focused on the positive effects on anabolic processes so far, mTOR also promotes growth by negatively regulating autophagy. Therefore mTORC1 directly suppresses 'unc-51 like autophagy activating kinase' Ulk, a kinase complex required to initiate autophagy.

Until today it has been well established that mTOR plays an important role in adipocyte differentiation^{11, 15}. mTOR signaling regulates adipocyte differentiation mainly by adjusting the cellular biosynthetic capacity to nutrient availability. On the one hand it has been shown that mTORC1 overactivation stimulates adipogenesis. On the other hand rapamycin-mediated mTORC1 inhibition down-regulates transcription factors such as C/ebp α and Pparg thereby decreasing the translation of proteins critical for adipogenesis. Whereas 4Ebp1 controls terminal differentiation *via* the master regulator Pparg, mTOR effector S6k1 regulates the expression of early adipogenic transcription factors. The mTORC1-mediated effect on adipogenesis has also been confirmed *in vivo*. Mice with adipose-specific loss of mTORC1 are lean animals with fewer and smaller adipocytes being resistant to high fat diet-induced obesity¹⁶. *In vivo* studies in humans showed that chronic nutrient overload activates mTOR signaling and leads to insulin resistance¹⁷, whereas inhibiting TOR-signaling in *Drosophila* blocks metabolic and cardiotoxic phenotypes caused by high fat diet¹⁸.

3.3 mTOR inhibition by rapamycin

In the early 1990s mTOR has been discovered as the physical target of rapamycin (*alias* sirolimus), a macrolide with anti-proliferative properties which has first been isolated from a soil sample of Rapa Nui island^{11, 19}. Rapamycin, which is produced by *Streptomyces hygroscopicus*, acts by complexing with the highly conserved immunophilin 'FK506 binding protein 12' (Fkbp12). Subsequently Fkbp12 binds and inhibits mTORC1, whereas mTORC2 acts rapamycin insensitive.

In clinical practice, rapamycin and its derivatives are mainly used in transplant patients due to their immunosuppressive activity. During treatments, weight loss which appears to be mTOR-associated has been observed in kidney transplant and kidney disease patients^{20, 21}. Nevertheless *in vivo* application of rapamycin and its derivatives in obese subjects for the purpose of inhibiting nutrient-driven mTOR overactivation and adipocyte differentiation is precluded by associated unfavorable side-effects on pancreatic islet cells, glucose homeostasis and insulin resistance²²⁻²⁴. Another disadvantage is that, after initial inhibition, 4Ebp1 becomes rapamycin-resistant in cells subjected to high dose or chronic rapamycin exposure resulting in sustained protein translation²⁵.

4. miRNAs in gene regulation

4.1 Biology of miRNAs

Whole genome sequencing in mammals revealed that 98 % of genetic material is non-coding RNA, which in part is involved in gene regulation^{26, 27}. MicroRNAs (miRNAs) are a group of highly conserved, 18-25 bp long noncoding RNAs that regulate gene expression in animals and in plants²⁸⁻³⁰. The first miRNA, namely lin-4, was discovered in 1993 in *Caenorhabditis elegans* by Victor Ambros and colleagues as a regulator of developmental timing. Ambros and Ruvkun groups noticed sequence complementarity between the short RNA product encoded by the lin-4 gene and the 3'-UTR of lin-14 mRNA. Further they described that this complementarity was necessary for LIN-14 protein translational inhibition and thereby discovered a new mechanism of gene regulation. In the following years growing numbers of small RNAs with regulatory roles were discovered and in 2001, this class of RNAs was termed 'microRNAs'. Until now, more than 1,800 human and 1,100 murine miRNAs have been identified (miRbase version 20). With the discovery of more of their respective targets and regulatory functions, the enormous biological impact of miRNA-mediated gene regulation became evident. MiRNAs are estimated to influence at least 30 % of genes in the human genome and it has been described that single miRNAs can control whole signaling cascades by targeting few key regulatory molecules within a given pathway³¹. As functional consequences miRNAs were shown to play major roles in a variety of biological processes and diseases including cell differentiation, proliferation and growth, apoptosis and cancer.

4.2 MiRNA biogenesis and mechanism of action

MiRNAs control gene expression post-transcriptionally through partial base-pairing with their target mRNAs, which leads to mRNA degradation or repression of translation²⁸⁻³⁰ (**Figure 3**).

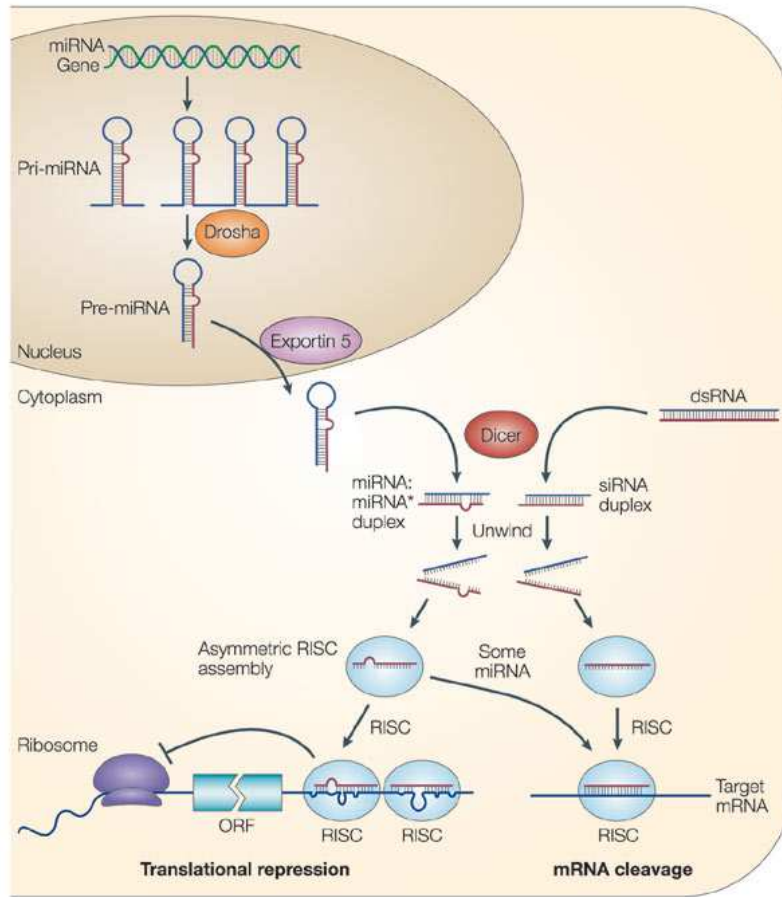


Figure 3: Current model for the biogenesis and post-transcriptional suppression of miRNAs

(from He *et al.*, Nature reviews³⁰).

Initially miRNAs are transcribed from their own genes, which are mainly found in intergenic regions or introns of protein-coding genes. The primary transcript of a miRNA gene (pri-miRNA) typically contains one or more hairpin structures and an imperfectly paired stem of approximately 30 bp with flanking 5'- and 3'-single stranded ends. The unique pri-miRNA structures are recognized and processed by the ribonuclease Drosha resulting in a RNA hairpin called pre-miRNA. While this pri-miRNA processing occurs in the nucleus, the nucleo/cytoplasmic transporter Exportin-5 (Exp-5) then transfers the pre-miRNA into the cytoplasm. Once inside the cytoplasm the pre-miRNA is cleaved by another ribonuclease complex called Dicer leading to miRNA:miRNA* duplex formation. The mature miRNA strand of the duplex is then incorporated into the 'RNA-induced silencing complex' RISC and induces target recognition whereas its complementary miRNA* strand is released and degraded. The subsequent recognition of target mRNAs

is based on the sequence complementarity of nucleotide positions 2–7 of the miRNA (named seed sequence) to its binding site, mostly located in the 3'UTR of a target gene. If perfect complementarity leads to target mRNA cleavage and central mismatches lead to repression of translation is an ongoing debate. However, miRNA-mediated mRNA degradation seems to be based on de-capping, de-adenylation and exonucleolytic digestion, whereas translation inhibition is poorly understood and may involve multiple mechanisms, such as inhibition of translation initiation and translation inhibition at the post-initiation stage²⁸⁻³⁰.

Interestingly, a study in humans showed that 37 % of the known miRNA genes appear in clusters of two or more miRNAs^{28, 32}. These miRNAs derive from a common multicistronic pri-miRNA and sometimes even show high sequence similarity. Clustered miRNAs are influenced by similar regulation mechanisms and thus they may regulate a common set of target mRNAs resulting in a functional relationship.

Further many mammalian miRNA genes were found to have paralogues that derived from gene duplication thereby forming miRNA families. Since paralogues often have identical seed sequences they may act redundantly³³.

4.3 MiRNAs in adipogenesis and nutrient sensing

Several high throughput studies have identified a number of miRNAs, which are de-regulated during mouse adipogenesis and some have also been experimentally validated as regulators of 3T3-L1 adipocyte differentiation³⁴. These include miR-143, miR-103 and cluster 17/92, which increase triglyceride accumulation and/or 3T3-L1 differentiation as well as miR-27a, let-7, miR-15a and miR-448, which attenuate 3T3-L1 differentiation. The mTOR pathway is well-characterized as a nutrient signaling pathway regulating cell differentiation. So far, however, only 3 miRNAs, namely miR-99a, -100 and -199a* have been confirmed to regulate mTOR signaling in the context of cancer and dermal wound healing³⁵⁻³⁸. Thus the pattern of miRNA regulation involved in mTOR signaling during adipocyte differentiation is not yet fully elucidated. A study of our group experimentally identified a set of mTOR-associated miRNAs and provides a list of their *in silico* predicted target genes within the mTOR pathway³⁹.

Some miRNAs, such as miR-103 and miR-107 were shown to play a role in obesity and its associated pathologies^{34, 40}. This knowledge has been transferred to treat e.g. hypercholesterolemia and liver steatosis in mice⁴¹, thereby demonstrating that miRNAs can provide a promising target class for novel therapeutic options.

5. Aims of the thesis

Understanding the molecular basis of nutrient-driven adipogenesis is essential to identify and monitor new therapeutics, either by drugs or diets that could ameliorate the adverse sequels of obesity. The identification of specific targets that exert rapamycin-like effects on nutrient signaling might provide an approach to search for alternative therapeutic options. In this study, we specifically aimed at identifying distinct miRNA-target pairs that are associated with the inhibition of adipogenesis *via* mTOR nutrient signaling. Specifically, the present study aimed at experimentally confirming selected miRNA-target pairs within the mTOR nutrient signaling pathway and at investigating candidate miRNAs' influence on adipocyte differentiation *via* the mTOR pathway.

B Material and Methods

1. Material

1.1 Sources of chemicals, reagents and enzymes

AppliChem, Darmstadt, Germany

Albumin Fraction V pH 7.0, NaN₃

Applied Biosystems, Carlsbad, USA

Nuclease-free water, Power SYBR® Green Mastermix, TaqMan® Universal PCR Master Mix

Aventis, Sanofi, Paris, France

Insulin *Insuman rapid* (40 I.E./ml)

Calbiochem® , Merck, Darmstadt Germany

Glycerol, Phosphatase Inhibitor Cocktail Set II, Protease Inhibitor Cocktail Set III

Carl Roth, Karlsruhe, Germany

Agar-Agar, Ampicillin, Bromphenol Blue, Isopropanol (≥99.8 %), MgSO₄, ATP, (MgCO₃)₄Mg(OH)₂, MgSO₄, sodium acetate, Tricine, Tris, Tween20

Fermentas, Waltham, USA

dNTPs, Gene Ruler™ 1 kb DNA Ladder, *NotI* restriction enzyme (Buffer 0), *Pfu*DNA Polymerase (*Pfu* buffer without MgSO₄), T4 DNA ligase (T4 DNA ligase buffer)

GIBCO, Carlsbad, USA

FBS

Invitrogen, Carlsbad, USA

Agarose, PBS, Lipofectamine™2000, DMSO

Merck, Darmstadt, Germany

NaCl

New England Biolabs, Beverly, USA

*Apa*I restriction enzyme (NEBuffer 4), *Asi*I restriction enzyme (NEBuffer 4)

PAA Laboratories GmbH, Pasching, Austria

Antibiotic-antimycotic solution, DMEM (4.5 g/L glucose, with L-Glutamin), Trypsin-EDTA (10x)

pjk, Kleinblittersdorf, Germany

Coenzym A, DTT

Qiagen, Hilden, Germany

Qiazol Lysis Reagent

Serva, Heidelberg, Germany

rapamycin stock (0.92mg/ml in DMSO)

Sigma-Aldrich, St. Louis, USA

7-AAD, Chloroform (>99 %), Dexamethasone 98 %, DMSO, EDTA, IBMX (1 M), LB Agar, Oil Red O stock (5 mg/ml), SDS, Triton X-100, Trypan Blue, 25 % glutaric acid

SynChem, Illinois, USA

coelenterazine, D-Luciferin

Thermo Fisher Scientific, Waltham, USA

Restore™ PLUS Western Blot Stripping Buffer

1.2 Buffers and solutions

<u>Flow cytometry Buffer</u>	2 %	FBS	
	0.02 %	NaN ₃	
<hr/>			
	ad PBS 500 ml		
<u>Laemmli Buffer 6x</u>	0.5 M	SDS	
	0.6 M	DTT	
	0.4 M	Tris	
	0.9 mM	Bromphenol Blue	
	9 M	Glycerol	
<hr/>			
	ad H ₂ O bidest. 50 ml	pH 6.8	

<u>Lysis Buffer 10x</u>	0.3 M	Tris	
	20 mM	Triton X-100	
	ad H ₂ O bidest. 400 ml		pH 7.4
<u>TBS-T Buffer 10x</u>	0.2 M	Tris	
	0.8 mM	Tween20	
	1.4 M	NaCl	
	ad H ₂ O bidest. 1 l		pH 7.6
<u>TNT Lysis Buffer 10x</u>	0.2 M	Tris	
	0.8 mM	Tween20	
	1.4 M	NaCl	
	ad H ₂ O bidest. 1 l		pH 7.4
<u>5 % BSA solution</u>	5 g	Albumin Fraction V	
	ad TBS-T buffer 1 l		pH 7.0
<u>Coelenterazine solution 5x</u>	0.05 mM	Coelenterazine (24 mM stock solution in MeOH)	
	ad H ₂ O bidest. 1 l		
<u>D-Luciferin solution</u>	0.5 mM	D-Luciferin	
	0.3 mM	Coenzym A	
	33 mM	DTT	
	0.6 mM	ATP	
	1 mM	(MgCO ₃) ₄ Mg(OH) ₂	
	5 mM	MgSO ₄	
	20 mM	Tricine	
	0.1 mM	EDTA	
	ad H ₂ O bidest. 1 l		

<u>0.5 % glutaric acid solution</u>	0.5 g	glutaric acid
	<hr/>	
	ad PBS 1 l	
<u>Oil Red O solution</u>	7.3 mM	Oil Red O
	<hr/>	
	ad H ₂ O bidest. 1 l	
<u>Rapamycin solution</u>	10 mM	rapamycin
	<hr/>	
	ad DMSO 1 ml	
<u>Sodium acetate solution</u>	3 M	sodium acetate
	<hr/>	
	ad H ₂ O bidest. 100 ml	pH 5.2

1.3 Plasmids and oligonucleotides

Ambion, Carlsbad, USA

Pre-miRTM miRNA Precursors, Pre-miRTM Negative Control #1, Anti-miRTM miRNA Inhibitors, Anti-miRTM Negative Control #1

Applied Biosystems, Carlsbad, USA

TaqMan[®] MicroRNA Assays

Invitrogen, Carlsbad, USA

pCR[®]_XL_TOPO[®] vector

Promega, Wisconsin, USA

psiCHECKTM-2 vector (**Figure S 1**)

Qiagen, Hilden, Germany

AllStars Negative Control siRNA AF488

Table 1: Oligonucleotide primer sequences and the respective cycling conditions and product sizes

Primers were designed using Primer3 software and synthesized by Metabion, Martinsried, Germany. Efficiency and specificity were tested for all primer pairs before use.

Gene	Sequence 5' → 3'	Optimal conditions	Size (bp)
<i>Pparγ</i>	CAG CAT TTC TGC TCC ACA CTA TGA AG	40 cycles 60.0°C	388
	AGC AAG GCA CTT CTG AAA CCG		
<i>Dlk1</i>	GAC CCA CCC TGT GAC CCC	40 cycles 60.0°C	757
	CAG GCA GCT CGT GCA CCC C		
<i>Pik3r1</i>	CCA AGC CCA CTA CTG TAG CC	45 cycles 60.0°C	171
	TGT AAT CGC CGT GCA TTT TA		
<i>Pik3r3</i>	TGA TGA TGC CCT ATT CGA CA	45 cycles 60.0°C	189
	CCC GCA ATT TGT CAT TTA CC		
<i>Tsc1</i>	CAAGCACCTCTTCTGCCTTC	45 cycles 60.0°C	194
	GTCACATGGCCTGGTTTCTT		
<i>Ppib</i>	TCC GTC GTC TTC CTT TTG	40/45 cycles 60.0°C	160
	CCA CTG TTT TTG GAA CAG TCT		
<i>Vegfa</i>	GTA CCT CCA CCA TGC CAA GT	40 cycles 60.0°C	183
	ACA CAG GAC GGC TTG AAG AT		
<i>Pik3r1</i> 3'UTR	Pho GTA GCGATCGC CTGCCCTCGGATCCAGTT	45 cycles 63.7°C	4,100
	GTA GCGGCCGC TTTTAAGTTTCAAACAACCTTTATTTC		
<i>Pik3r3</i> 3'UTR	Pho GTA GCGATCGC GCAGAGTGAAGAGACACGCT	45 cycles 65.6°C	3,200
	GTA GCGGCCGC TTCCTGCAATGTCTTTATTGCATC		
<i>Tsc1</i> 3'UTR	Pho GTA GCGATCGC GGTCTGTCAGTGTTCAATTTGC	45 cycles 57.7°C	4,000
	GTA GCGGCCGC GCAAACAATAAATCTTTATTGTTCA		

1.4 Antibodies

Cell Signaling Technology, Danvers, USA

AKT1 (C73H10), α -tubulin (11H10), Hamartin/TSC1 (D43E2), p70 S6 Kinase (49D7), Phospho-p70, S6Kinase (Thr389), PI3 Kinase p85 (19H8)

Thermo Fisher Scientific, Waltham, USA

RSK3

1.5 Commercial kits

Applied Biosystems, Carlsbad, USA

TaqMan[®] MicroRNA RT Kit

BioRad, Hercules, USA

Immun-Star[™] HRP Chemiluminescent Kit

Macherey-Nagel, Düren, Germany

NucleoSpin[®] Extract II Kit

Thermo Fisher Scientific, Waltham, USA

Pierce[®] BCA Protein Assay Kit

Qiagen, Hilden, Germany

miRNeasy[®] Mini Kit, QIAprep[®] Miniprep Kit, QuantiTect[®] Reverse Transcriptase Kit

1.6 Cell lines

Invitrogen, Carlsbad, USA

ElectroMAX[™] DH10B[™] cells

LGC Standards, Teddington, UK

HEK-293 cells (ATCC[®] CRL-1573[™]), 3T3-L1 cells (ATCC[®] CL-173[™])

1.7 Consumables

Applied Biosystems, Carlsbad, USA

MicroAmp optical 96-well reaction plates

BioRad, Hercules, USA

GenePulser[®] electroporation cuvette

Corning, New York, USA

Corning[®] 175 cm² Flask, Costar[®] 6-well cell culture plate

Eppendorf, Hamburg, Germany

PCR Tubes 0.2 ml, Safe-Lock Tubes 1.5 ml, Safe-Lock Tubes 2.0 ml

GE Healthcare, Little Chalfont, UK

Amersham Hybond[™]-P PVDF Membrane

Thermo Fisher Scientific, Waltham, USA

LumiNunc F96, Nunclon[™] Surface 24-well plates, Nunclon[™] Surface 96-well plates

1.8 Equipment and software

Applied Biosystems, Carlsbad, USA

7900HT Fast Real-Time PCR System, SDS software 2.3 2005

Becton Dickinson, San Jose, USA

BD FACSCanto™ Flow Cytometer, BD FACSDiva™ software v. 5.0.3

BioRad, Hercules, USA

Gene Pulser II, mini-PROTEAN® Tetra System

BMG Labtech, Ortenberg, Germany

FluoStar OPTIMA luminometer, FluoStar OPTIMA software

BSRC Alexander Fleming, Athens, Greece

DIANA-miRPath v.1.0

Eppendorf, Hamburg, Germany

Thermomixer comfort

GraphPad Software, San Diego, USA

GraphPad PRISM® v. 5.0.1

Innovatis, Bielefeld, Germany

Cellscreen

Leica Microsystems, Wetzlar, Germany

Leica DMIL microscope

Microsoft, Redmond, USA

Microsoft Office Professional Plus 2010

New Brunswick Scientific, Nürtingen, Germany

Excella E24 Incubator Shaker

NIH, Maryland, USA

ImageJ

PEQLAB Biotechnologie GmbH, Erlangen, Germany

96 Universal Gradient peqSTAR

Qiagen, Hilden, Germany

QIAcube RNA Purification roboter

Scientific Industries, New York, USA

Vortex Genie 2

Thermo Fisher Scientific, Waltham, USA

HERAcell 240 incubator, Heraeus Fresco 17 Centrifuge, Nanodrop® MD-1000

Universität Düsseldorf, Düsseldorf, Germany

Ligation Calculator

Whitehead Institute for Biomedical Research

Primer3 v. 0.4.0

2. Methods

2.1 *In silico* target prediction

Prediction of direct miRNA targets was performed using five prediction programs: PITA, miRanda, targetScanS, pictar and targetspy. Targets with consensus target prediction of at least 2 algorithms were considered predicted. Because of the similarity of their seed sequences, miRNAs belonging to the same family were grouped. For pathway enrichment analysis, DIANA-miRPath (v.1.0) software was used applying PicTar 4-way and TargetScan 5 algorithms⁴².

2.2 Luciferase reporter assay

3'UTR amplification

3'UTRs of the target genes *Pik3r1*, *Pik3r3* and *Tsc1* were PCR-amplified according to following experimental protocols (**Table 2**).

Table 2: Thermal cycling conditions for 3'UTR amplification of target genes *Pik3r1*, *Pik3r3* and *Tsc1*

95 °C	10 min	Initial denaturation	
95 °C	30 s	Denaturation	45 cycles
63.7°C (<i>Pik3r1</i>) 65.6°C (<i>Pik3r3</i>) 72.0°C (<i>Tsc1</i>)	30 s	Primer annealing	
72 °C	4 min 30 s	Elongation	
72 °C	10 min	Final elongation	

Amplification was performed using primer pairs spanning complete 3'UTRs (primer sequences are given in section 0) and *Pfu* DNA Polymerase on a 7900HT FastRealTime PCR Cycler and analyzed using SDS software 2.3 2005.

Table 3: Optimized reaction setups for 3'UTR amplification of target genes *Pik3r1*, *Pik3r3* and *Tsc1*

volume [μ l]	reagent	final concentration
2.5 μ l	<i>Pfu</i> Buffer without MgSO ₄ (10x)	1x
1 μ l	dNTPs (10 mM)	2.5 mM
1 μ l	BSA (100x)	4x
3 μ l (<i>Pik3r1</i> , <i>Pik3r3</i>) 2 μ l (<i>Tsc1</i>)	MgSO ₄ (25 mM)	3 mM/2 mM
2 μ l	<i>Pfu</i> DNA Polymerase (2.5 U/ μ l)	5 U
0.5 μ l	Primer fwd (100 μ M)	2 μ M
0.5 μ l	Primer rev (100 μ M)	2 μ M
2 μ l (<i>Pik3r1</i> , <i>Tsc1</i>) 3 μ l (<i>Pik3r3</i>)	mouse genomic DNA (80 ng/ μ l)	160ng/240 ng
12.5 μ l (<i>Pik3r1</i>) 11.5 μ l (<i>Pik3r3</i>) 13.5 μ l (<i>Tsc1</i>)	nuclease-free water	

Cloning

Amplified 3'UTRs of *Pik3r1*, *Pik3r3* and *Tsc1* were purified by excision from agarose gel using NucleoSpin[®] Extract II Kit and cloned into pCR[®]_XL_TOPO[®] vector followed by sub-cloning into psiCHECK[™]-2 vector (**Figure S 1**). TOPO TA cloning[®] is a one-step cloning strategy for the direct insertion of PCR-products into pCR[®]_XL_TOPO[®] vector without digestion or ligation reactions. TOPO TA cloning[®] was performed according to manufacturer's instructions. For subsequent cloning into the *NotI* and *AsiI* restriction site of psiCHECK[™]-2 vector, restriction enzyme digestions were performed using 5 μ l of specific 10x buffer, 0.5 μ l 100x BSA, 0.2 μ l of enzyme (10 U/ μ l) and 1-2 μ g DNA in a 50 μ l reaction volume. Digestions were run at 37°C for at least 4 h and then cleaned-up using NucleoSpin[®] Extract II Kit. Complete 3'-UTRs were ligated into 100 ng psiCHECK[™]-2 reporter plasmid using T4 DNA ligase (5 U/ μ l) following manufacturer's instructions. Exact amounts of inserts were determined by "ligation calculator software" calculating the exact volumetric ratio (1:3) between vector and insert in the ligation

reaction. In order to verify the identity of the cloned insert, digestions using *Apa*LI according to manufacturer's guidelines were set up for an analytical agarose gel. To purify and concentrate vector constructs, chloroform precipitation was used as described in section B 2.5.

In order to amplify the vector constructs electrocompetent *E.coli* cells were transformed by electroporation. For this purpose, 2 µl of electrocompetent *E.coli* were added to 50 and 100 ng plasmid vector in 50 µl nuclease-free water. The mixtures were transferred to a pre-cooled GenePulser® electroporation cuvette and transformation was performed on a Gene Pulser II using the following conditions: 1,800 V, 100 Ω, 25 µF. The mixtures were pipetted into pre-warmed LB medium directly after electroporation and incubated at 37°C for 1 h, followed by centrifugation at 4,000 rpm for 4 min. Subsequently the supernatant was discarded and the pellet was resuspended in the remaining liquid. 50 µl and 100 µl of resuspension was spread on LB-Amp¹⁰⁰ agar plates (15 g Agar-Agar in 1 l LB medium) and cultured at 37°C overnight. Formed colonies were picked and transferred to 5 ml LB-Amp¹⁰⁰ overnight cultures incubated at 37°C. For plasmid purification QIAprep® Miniprep Kit was applied following manufacturer's instructions. Clones were verified by control digestion with *Apa*LI.

Measurement of reporter gene expression

Direct interaction between the candidate miRNAs and the 3'-UTRs of the predicted target genes *Tsc1*, *Pik3r1* and *Pik3r3* was examined by luciferase-based reporter assays. Therefore HEK-293 cells, cultured in DMEM (4.5 g/L glucose, with L-Glutamin) supplemented with 10 % heat-inactivated FBS and 1 % antibiotic-antimycotic solution in 24-well plates, were transfected using Lipofectamine2000 according to the manufacturer's instructions. 20 pmol of the respective Pre-miRTM miRNA Precursor or negative control #1 and 100 ng of the reporter vector-3'UTR constructs were co-transfected per well.

In case of effective silencing by the respective miRNAs *Renilla* luciferase activity is reduced due to the adjacently inserted 3'UTR. Firefly luciferase activity was used as a control for transfection efficiency. *Renilla* luciferase activity was quantified using coelenterazine as substrate whereas firefly luciferase activity was quantified by addition of its substrate luciferin. Therefore cells were lysed 72 h after transfection by addition of 120 µl lysis buffer per well and incubated for 10 min at room temperature with constant agitation. Using a white 96-well plate, 100 µl of the respective substrate solutions were added automatically to 50 µl of lysed sample and luminescence was measured by

FluoStar OPTIMA luminometer. Background luminescence was subtracted for each well by FluoStar software. Subsequently, *Renilla* luciferase activity was normalized to firefly luciferase activity for each sample. Luciferase assay was performed in two independent experiments each performed in triplicates.

2.3 Transfection experiment

Culture of 3T3-L1 adipocytes

For transfection and differentiation experiments, 3T3-L1 cells were pre-cultured in DMEM (4.5 g/l glucose) supplemented with 10 % heat-inactivated FBS and 1 % antibiotics/antimycotics at 37°C and 5 % CO₂ under standard conditions. Detachment of cells was achieved by addition of 2 ml Trypsin-EDTA (0.05 % (w/v) Trypsin and 0.5 mM EDTA) per 175 cm² cell culture flask and subsequent incubation for 4 min at 37°C. As soon as detachment was visible, cell culture medium was added to stop the enzymatic reaction.

Transfection

For transfection, cells were seeded in 24-well plates (80,000 cells per well). After 24 hours cells reached confluence and transfection was performed using Lipofectamine2000 following manufacturer's instructions. 20 pmol of the respective Pre-miRTM miRNA Precursors and or Anti-miRTM miRNA Inhibitors were transfected. Cells transfected with Pre-miRTM miRNA Precursor Negative Control #1 or Anti-miRTM miRNA Inhibitor Negative Control #1 were used as control.

Cell harvest

After 3 days, cells were harvested by adding 200 µl Qiazol Lysis Reagent and incubated at 37°C for 2 minutes. Four independent experiments were performed, with each treatment done in 6 replicates, which were pooled. RNA was isolated and miRNA- as well as mRNA levels were quantified as described in section B 2.5. Harvesting of cells for immunoblots is described in section B 2.6.

2.4 Differentiation experiment

Cell culture and transfection

3T3-L1 adipocytes were pre-cultured as for transfection experiments. For differentiation experiments, cells were seeded in 6-well plates (250,000 cells/well). After 24 hours cells were transfected with 80 pmol pre-/anti-miRNAs using Lipofectamine2000 as described

in section B 2.3. Cells transfected with negative control pre-/anti-miRNAs were used as control.

Differentiation

Two days after transfection, differentiation was initiated (designated as day 0) by the addition of 200 nM insulin, 1 μ M dexamethasone and 0.5 mM IBMX to growth medium. After 3 days cells were further grown in growth medium supplemented with 200 nM insulin and medium was changed again at day 5. A rapamycin concentration of 20 nM directly added to the medium was used for inhibition of 3T3-L1 adipogenic differentiation. Cells were visually monitored for viability during the whole procedure.

Cell harvest

Cells were harvested at day 0, day 3 and day 6 of differentiation by the addition of 750 μ l Qiazol Lysis Reagent per well. Two independent experiments were performed, each measured in technical triplicates. RNA was isolated and miRNA- as well as mRNA levels were quantified as described for transfection experiments.

Lipid droplet quantification

Oil Red O staining of 3T3-L1 adipocytes was performed following the procedure described by Green and Kehinde⁴³ with minor modifications. Briefly, cells were washed with PBS and fixed in 0.5 % glutaric acid solution for 5 min. Cells were washed twice with PBS followed by a wash step with 60 % isopropanol. Cells were stained in freshly prepared Oil Red O solution for 1 h. After staining, the cells were subsequently washed with 60 % isopropanol and PBS. Quantification of lipid droplet size (μm^2) and number was evaluated optically by light microscopy at day 6 of differentiation using a digital image analysis approach as previously described⁴⁴. For this purpose, Oil Red O stained cell images were thresholded for the lipid droplet signal *via* imaging software ImageJ. In order to identify single droplets and separate overlapping droplets the image was subjected to watershed object separation. Data were exported and analyzed using Microsoft Excel software.

In a second confirmatory approach, lipid droplets were quantified by an absorbance based method. Therefore cells were de-stained with 100 % isopropanol for 30 minutes and the Oil Red O content in the supernatant was measured by FluoStar OPTIMA luminometer. Absorbance was normalized to the percentage of well area covered by cells as determined using Cellscreen automated microscopy.

2.5 RNA/DNA analysis

Isolation of total RNA including small RNAs

For total RNA-isolation, 3T3-L1 cells were lysed directly by adding QIAzol Lysis Reagent. Lysates were transferred into a microcentrifuge tube and cooled on ice until RNA was isolated with miRNeasy Mini Kit and QIAcube RNA Purification roboter according to manufacturer's instructions.

Chloroform precipitation for DNA purification

Vector constructs were purified and concentrated after ligation reaction as followed: An equal volume of chloroform was added to the sample and the tube was mixed vigorously until an emulsion was formed. The aqueous phase was transferred to a fresh tube, while the organic and interphase were discarded. For DNA precipitation 0.3 M final concentration of sodium acetate pH 5.2 and two volumes of 100 % ethanol were added. Samples were incubated at -20°C for 1 h and subsequently centrifuged at 4°C for 30 min. After removal of the supernatant, the pellet was washed once with 70 % ethanol, air-dried and resuspended in 10-50 µl aqua *ad injectabilia*.

RNA Quality testing

RNA quality and concentration was determined by absorbance measurement. Acceptable values were defined as 260/280 nm ratios above 2.0 and 260/230 nm ratios above 1.0. In addition, RNA integrity was analyzed by native agarose gel electrophoresis. Therefore, 1-3 µg RNA was denatured at 85°C for 3 min. After cooling on ice and addition of 2 µl loading dye, samples were loaded on a 0.8 % agarose gel in TAE buffer with 0.5 µg/ml ethidium bromide added to the gel and run at 75 V.

miRNA analysis

For miRNA quantification, RNA was reverse transcribed and subjected to real-time PCR (rt-PCR) analysis. Therefore cDNA synthesis from 50 ng total RNA was performed using TaqMan® MicroRNA RT Kit (Applied Biosystems) and TaqMan® MicroRNA Assay RT Primer according to manufacturer's instructions on a 96 Universal Gradient peqSTAR. Components for subsequent rt-PCR reaction were 3.3 ng cDNA, 1x respective TaqMan® MicroRNA Assay PCR Primer and 1x TaqMan® Universal PCR Master Mix. Total reaction volume was 15 µl. Reactions were run in triplicates on a 7900HT Fast Real-Time PCR System (Applied Biosystems) following the thermal profile in **Table 4**. "Non-template" controls were included.

Table 4: Thermal cycling conditions for miRNA quantification

95 °C	3 min	Initial denaturation	
95 °C	15 s	Denaturation	45 cycles
60 °C	1 min	Primer annealing & elongation	
95 °C	10 min	Final denaturation	

Small nucleolar RNAs (snoRNAs) are commonly used reference genes for miRNA expression analyses⁴⁵. Two different snoRNAs, namely sno-202 and sno-234 were tested in the present experimental settings. Sno-202 showed more stable transcriptional expression and thus was used as reference gene. Relative quantification was calculated by $\Delta\Delta C_T$ -method⁴⁶.

mRNA analysis

For relative quantification of gene expression, RNA was reverse transcribed and quantified by real-time PCR analysis. Therefore 400 ng total RNA were reverse transcribed on a 96 Universal Gradient peqSTAR using QuantiTect[®] Reverse Transcriptase Kit following manufacturer's instructions. For rt-PCR, 25 μ l-reactions consisting of 1 μ l cDNA, 500 nM forward and reverse primer (**Table 1**), 12.5 μ l 2x Power SYBR[®] Green Mastermix containing SYBR[®] Green I Dye, AmpliTaq Gold[®] DNA Polymerase, dNTPs, passive reference (ROX) and optimized buffer components were subjected to the following experimental run protocol (**Table 5**) on a 7900HT Fast Real-Time PCR System. Reactions were run in triplicates and "non-template" controls were included. Melting curve analysis confirmed specific amplification.

Table 5: Thermal cycling conditions for transcript quantification

95 °C	3 min	Initial denaturation	
95 °C	15 s	Denaturation	45 cycles
60 °C	1 min	Annealing & elongation	
95 °C	30 sec	Final denaturation	
55°C	30 sec		
55-95 °C	10 sec	Melting curve	80 repeats

Transcriptional stability of five commonly used reference genes *Ppib*, ubiquitin-conjugating enzyme E2D 2A *Ube2d2*, hypoxanthine guanine phosphoribosyl

transferase *Hprt*, beta actin *Actb*, 18S ribosomal RNA *Rn18s*), was evaluated in the present experimental settings⁴⁷. Results indicated that *Ppib*, encoding for cyclophilin B protein, was the most stable internal control gene in this study. Hence, data were normalized to the reference gene *Ppib* and analyzed using $\Delta\Delta C_T$ -method⁴⁶.

2.6 Immunoblot analysis

Protein lysates and quantification

Protein extracts were collected from 3T3-L1 cells 72 hours *post* Pre-miRTM miRNA Precursors/Anti-miRTM miRNA Inhibitors transfection. Cells were scraped in 400 μ l pre-cooled TNT lysis buffer supplemented with Protease (5 μ l/ml) and Phosphatase Inhibitor Cocktails (10 μ l/ml). After double thaw and re-freeze lysates were centrifuged at 13,300 rpm for 20 min at 4°C. Protein concentrations of clear supernatants were determined using BCA protein assay with bovine serum albumin as standard according to manufacturer's instructions.

Immunodetection

Equal amounts of protein from cleared lysates were denatured by incubation at 99°C for 5 minutes in Laemmli buffer and subsequently separated (10 μ g/lane) on a 10 % SDS-polyacrylamide gel with the mini-PROTEAN electrophoresis module assembly. After blotting on a PVDF membrane, the membrane was incubated for 1 h at room temperature in 5 % BSA and immunoreacted overnight at 4°C with the respective rabbit anti-mouse antibodies against Phospho-p70 S6 Kinase (1:1,000), p70 S6 Kinase (1:2,000), Hamartin/Tsc1 (1:1,000), PI3 Kinase p85 (1:1,000), Rsk3 (1:4,000), Akt1 (1:1,000) and α -Tubulin (1:1,000). Using anti-rabbit IgG HRP-linked antibody (1:2,000) proteins were immunodetected by Immun-StarTM HRP Chemiluminescent Kit. In order to normalize the observed protein signals to the applied protein amount, membranes were stripped with RestoreTM PLUS Western Blot Stripping Buffer for 30 min at 37°C and re-stained using an anti- α -Tubulin antibody (1:2,000). Blots were quantified by ImageJ using a digital image analysis approach.

2.7 Flow cytometry analysis

For determining transfection efficiencies and cell viability, 3T3-L1 pre-adipocytes were transfected with labelled AllStars Negative Control siRNA AF488 (Qiagen). Cells were trypsinized and harvested by adding 500 μ l growth medium per well. After a washing-step in PBS, cells were resuspended in flow cytometry buffer (10 % FBS in PBS). Cell viability was determined by staining cells with 7-AAD. A working solution of 0.05 μ g/ml

7-AAD in PBS was prepared and 5 μ l were added to a cell suspension of 1 million cells following incubation at room temperature for 7 min. A BD FACSCanto™ flow cytometer was used to analyze both, cell viability and transfection efficiencies. 10,000 cells were measured for each treatment group. Data were collected and analyzed by BD FACSDiva™ software.

2.8 Statistical analysis

Statistically significant differences of quantitative PCR and reporter assays were evaluated using Student's *t*-test provided in GraphPad Prism 5.0 (GraphPad Software, San Diego, CA, USA). *P* values of 0.05 or less were considered significant. * indicates $P \leq 0.05$, ** $P \leq 0.01$ and *** $P \leq 0.001$.

C Results

1. 3T3-L1 adipocyte model characterization

Differentiation of 3T3-L1 pre-adipocytes (day 0) into adipocytes (day 6) was evaluated by increased levels of the adipocyte marker transcript *Ppar γ* (15-fold, $P = 0.073$) and decreased levels of pre-adipocyte marker transcript *Dlk1* (*alias Pref-1*; 4-fold, $P = 0.016$, **Figure 4A**). Further increasing deposition of lipid droplets was confirmed by Oil Red O staining (**Figure 4B**).

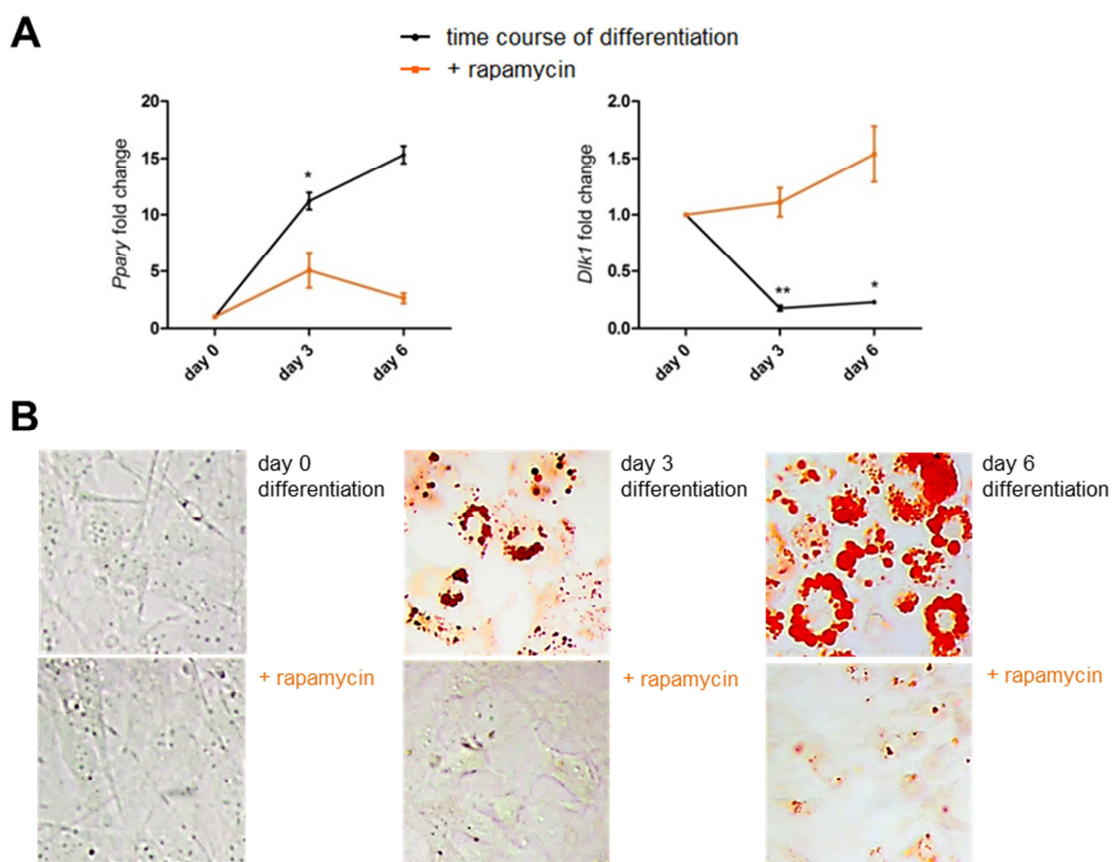


Figure 4: Inhibitory effects of rapamycin on 3T3-L1 adipogenic differentiation

(A) Quantification of adipocyte marker *Ppar γ* gene expression and pre-adipocyte marker *Dlk1* (*alias Pref-1*) gene expression in untreated (differentiation) and rapamycin-treated (+ rapamycin) cells undergoing a differentiation protocol for 6 days. Mean values \pm S.E.M. of 2 experiments, each performed in technical triplicates. **(B)** Phenotypic comparison of untreated and rapamycin-treated cells undergoing a differentiation protocol for 6 days. Cells were fixed and stained with Oil Red O (200x magnification).

* $P \leq 0.05$, ** $P \leq 0.01$

The expression of marker genes in rapamycin-treated adipocytes resembled pre-adipocytes at early stage of differentiation. Additionally, a markedly decreased cytoplasmic lipid droplet accumulation compared to mature adipocytes was observed ($P = 0.012$, **Figure 4**).

2. *In silico* target prediction

A study of our group experimentally identified a set of 22 candidate miRNAs associated with both, adipocyte differentiation and mTOR nutrient signaling³⁹. Discovering the targets of these miRNAs is essential to unravel their regulatory function. A stringent *in silico* target prediction approach using five different algorithms revealed that 16 miRNAs, which previously showed rapamycin dependent expression changes in differentiation experiments, were also predicted to target mTOR pathway genes (**Table S 1**). Relationship upstream and downstream of the predicted mTOR targets to mTOR complex 1 is shown in **Figure 5**.

Further molecular pathways being altered by the set of rapamycin-sensitive miRNAs were identified using the computational pathway-prediction tool DIANA-miRPath. Pathway enrichment analysis revealed that the *in silico* predicted targets were significantly enriched in the mTOR pathway ($P_{\text{PicTar 4-way}} = 1.95\text{E-}03$, $P_{\text{TargetScan5}} = 5.41\text{E-}03$) and other mTOR-related pathways such as insulin signaling ($P_{\text{PicTar 4-way}} = 7.23\text{E-}07$, $P_{\text{TargetScan5}} = 1.90\text{E-}03$) or MAPK signaling pathway ($P_{\text{PicTar 4-way}} = 3.01\text{E-}09$, $P_{\text{TargetScan5}} = 1.53\text{E-}09$).

A subset of five miRNA-target pairs, namely miR-183 - *Tsc1*, miR-378 - *Tsc1*, miR-103 - *Pik3r1*, miR-107 - *Pik3r1* and miR-182 - *Pik3r3* were subsequently selected for confirmation of direct miRNA-target interaction. Selection criteria were significant rapamycin effects on 3T3-L1 adipogenic differentiation, prediction of targets that are central genes of the mTOR pathway and/or members of miRNA clusters and families. Rapamycin-sensitive expression of these miRNAs was first reproduced and indeed confirmed in the current experimental setting (**Figure S 2**).

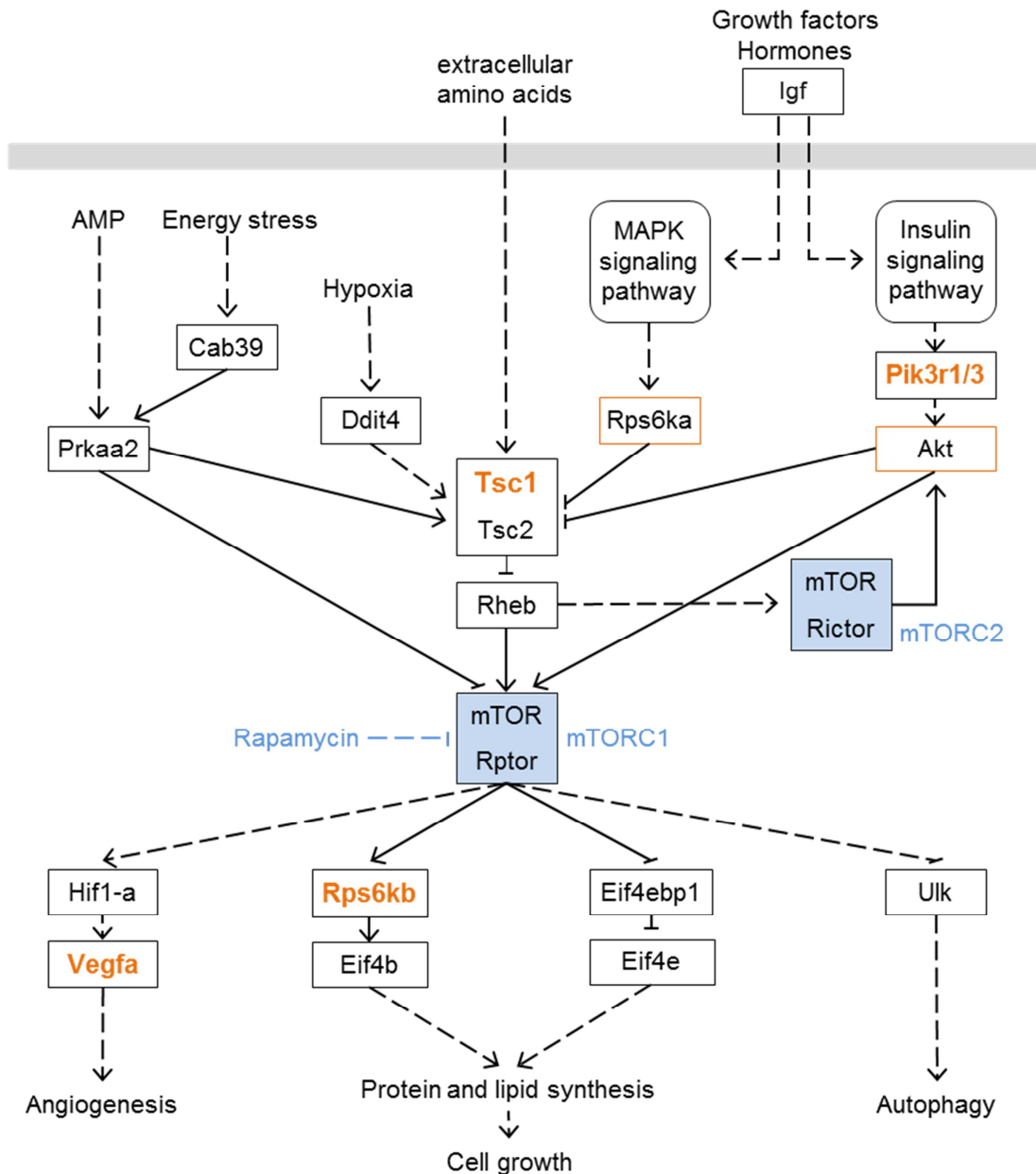


Figure 5: *In silico* prediction of miRNA targets within mTOR signaling pathway

→ molecular interaction or activation, —| inhibition, -→ indirect effect. Predicted target genes of rapamycin-sensitive miRNAs within mTOR signaling pathway (Table S 1) are depicted. mTOR complex 1 (mTORC1) and mTOR complex 2 (mTORC2) are blue-shaded. *Tsc1*, *Pik3r1* and *Pik3r3* genes (encode two different subunits of Pi3k protein) were predicted targets of miRNA candidates chosen for further investigation. *Rps6kb* (protein name S6k1) and *Vegfa* were used for evaluating mTOR output. *Rps6ka* (protein name Rsk) and Akt were investigated as candidate targets upstream Tsc1.

3. Functional validation of miRNA-target gene pairs

To assess binding of the selected miRNAs to the 3'UTR of their target genes, luciferase-based reporter assays were performed. HEK-293 cells were co-transfected with the respective Pre-miRTM miRNA Precursor molecules and bi-cistronic reporter plasmids harboring the 3'UTRs of predicted miRNA target genes. A significantly reduced luciferase activity indicated binding of miR-183 and miR-378 to *Tsc1* 3'UTR ($P < 0.0001$ and $P = 0.0013$; **Figure 6A**) and of miR-103 to *Pik3r1* 3'UTR ($P = 0.0022$; **Figure 6B**). MiR-107 and miR-182 were not detected to bind to the 3'UTRs of their predicted target genes *Pik3r1* and *Pik3r3* respectively (**Figure 6B and C**).

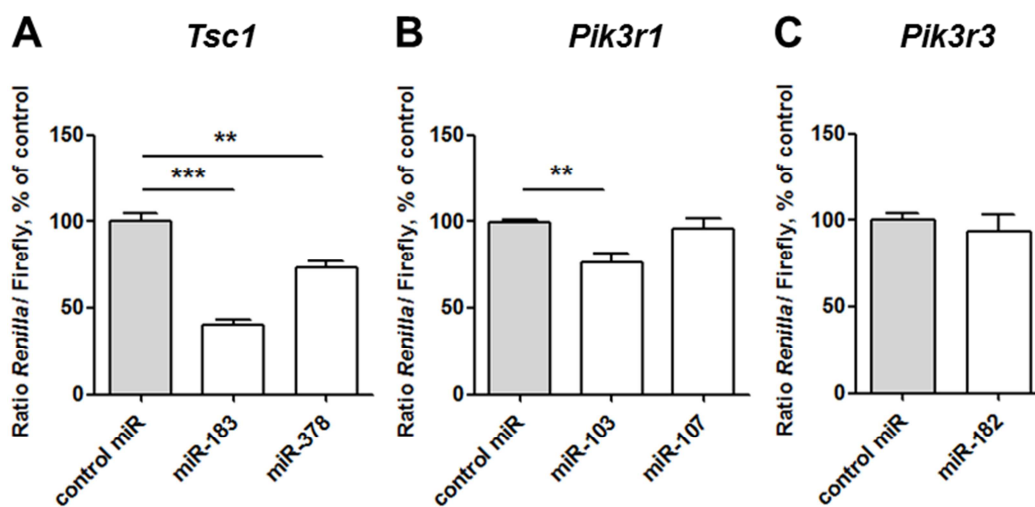


Figure 6: MiRNA binding to the 3'UTRs of predicted target genes

Relative luciferase expression of HEK-293 cells transfected with Pre-miRTM miRNA Precursor miR-183, -378, -103, -107 or -182 and a luciferase reporter plasmid harbouring the 3'UTRs of predicted target genes **(A)** *Tsc1*, **(B)** *Pik3r1* and **(C)** *Pik3r3*. Mean values \pm S.E.M. of 2 independent experiments performed in technical triplicates.

** $P \leq 0.01$, *** $P \leq 0.001$

To investigate miRNA-mediated down-regulation of the respective target gene expression, 3T3-L1 pre-adipocytes were transfected with Pre-miRTM miRNA Precursor molecules.

For assay establishment 3T3-L1 cells were transfected with AF488 labelled oligonucleotides and transfection efficiencies as well as cell viability were measured via flow cytometry for various experimental conditions. Survival rates were between 86 %

and 92 % depending on concentration of transfected siRNA and the selected time point (**Figure S 3**). Flow cytometry analysis showed that percentage of transfected cells decreased with time after transfection procedure: Transfection was successful in 71 % ($P = 0.0015$) of cells transfected with 20 pmol of labelled siRNA after 24 hours, 69 % ($P = 0.0058$) after 48 hours and 51 % ($P = 0.0026$) after 72 hours (**Figure 7A, Figure S 4**). Transfection efficiency increased with rising concentrations of siRNAs: Cells transfected with 10 pmol labelled siRNA per well showed a transfection efficiency of 59 % ($P = 0.0027$), with 20 pmol 71 % ($P = 0.0014$) and with 40 pmol 86 % ($P = 0.0001$) when harvested 24 hours *post* transfection (**Figure 7A, Figure S 5**). Flow cytometry results were confirmed by rt-PCR. As depicted for miR-378 and miR-183, up-regulation of intracellular miRNA levels slightly decreased after 48 and 72 hours and increased with rising miRNA-concentrations that were transfected (**Figure 7**). In subsequent experiments cells were transfected with 20 pmol of the respective miRNAs and then harvested 72 hours *post* transfection. The increase in the individual intracellular miRNA levels measured *via* rt-PCR 72 hours *post* transfection is shown in **Figure 7C**.

MiRNA-mediated target mRNA down-regulation was assessed *via* rt-PCR. *Tsc1* transcript levels were down-regulated significantly in miR-183 ($P = 0.0044$) and miR-378 transfected cells ($P < 0.0001$; **Figure 8A**). MiR-103 transfection resulted in significant down-regulation of *Pik3r1* gene expression levels ($P < 0.0001$; **Figure 8B**). No down-regulation of the predicted target gene *Pik3r1* and *Pik3r3* expression levels was observed in cells transfected with miR-107 and miR-182 (**Figure 8B and C**).

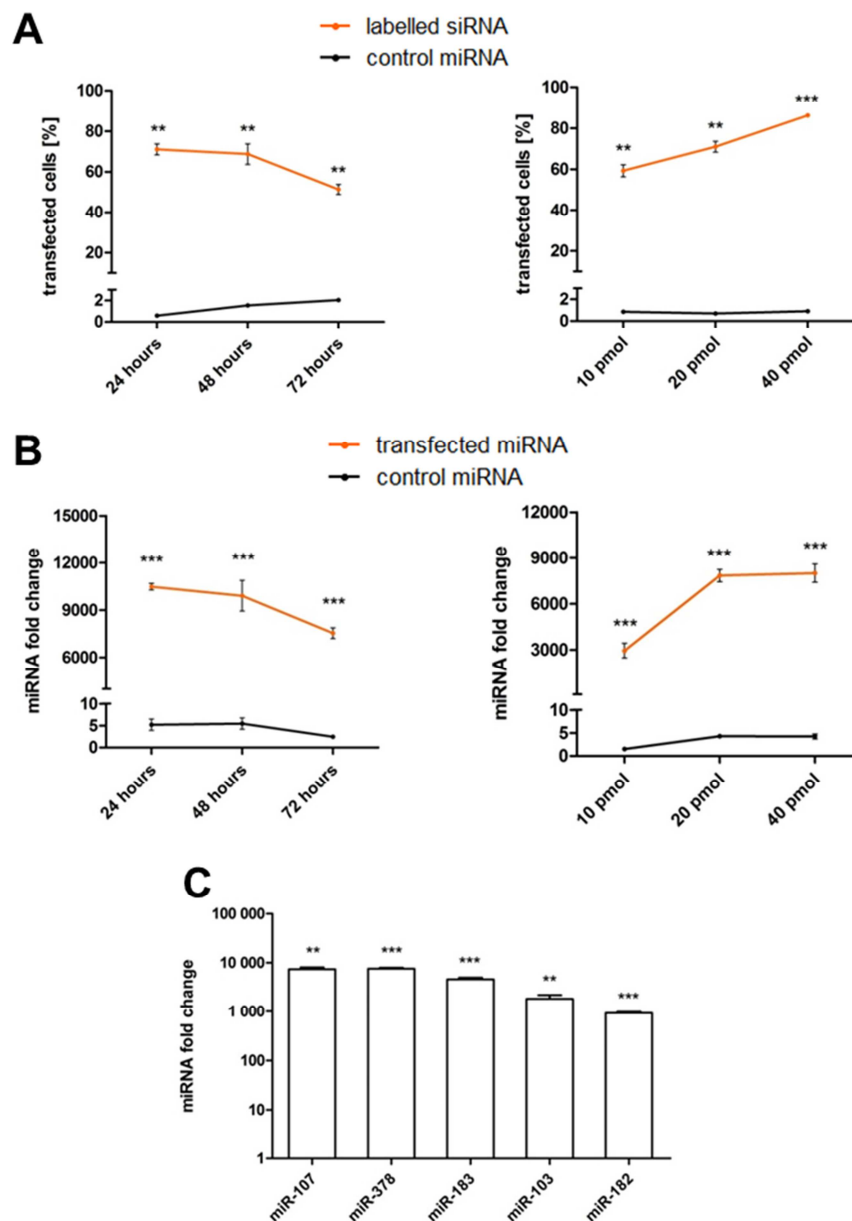


Figure 7: Time course and concentration-dependency of intracellular miRNA increase after transfection

(A) Percentage of transfected 3T3-L1 pre-adipocytes measured by flow cytometry at different time points *post* transfection and in cells transfected with different concentrations of labelled siRNA. **(B)** Time course and concentration dependency of miRNA increase after transfection with a candidate Pre-miRTM miRNA quantified by rt-PCR. **(C)** Intracellular miRNA levels after transfection with 20 pmol of the respective Pre-miRTM miRNA measured *via* rt-PCR 72 hours *post* transfection. Mean values \pm S.E.M. of 2 independent experiments being performed in 6 well replicates. ** $P \leq 0.01$, *** $P \leq 0.001$

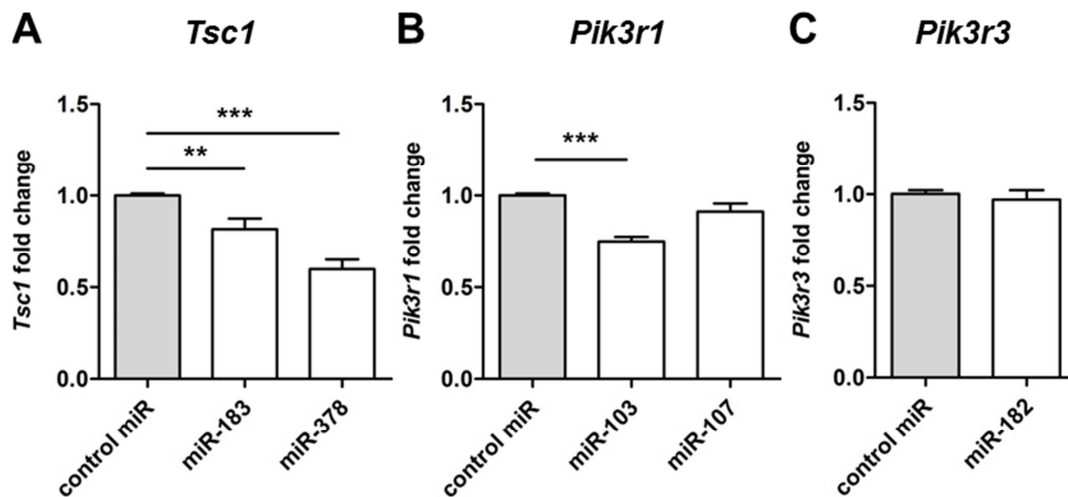


Figure 8: MiRNA-mediated down-regulation of target transcripts

Gene expression levels of *Tsc1*, *Pik3r1* and *Pik3r3* were quantified using rt-PCR in 3T3-L1 pre-adipocytes transfected with the respective Pre-miRTM miRNA Precursor or Control molecules 72 hours *post* transfection. Mean values \pm S.E.M. of 4 independent experiments performed in 6 well replicates. ** $P \leq 0.01$, *** $P \leq 0.001$

To assess miRNA-mediated effects on target protein levels, immunoblots were performed from 3T3-L1 pre-adipocytes transfected with Pre-miRTM miRNA Precursor molecules. *Tsc1* (*alias* hamartin) protein levels showed a slight increase in cells transfected with miR-183 (36 %, $P = 0.30$) or miR-378 (40 %, $P = 0.50$). However, *Pik3r1* protein levels did not change in miR-103 or miR-107-transfected adipocytes (**Figure 9**).

4. MiRNA-mediated regulation of mTOR effectors

mTORC1 has been described to regulate protein synthesis *via* phosphorylation of S6k1 and to promote angiogenesis by Hif1a-mediated stimulation of *Vegf* gene expression⁴⁸. Thus miRNA effects on mTOR signaling were evaluated by measuring phosphorylation of S6k1 and by determination of *Vegf* gene expression levels in 3T3-L1 pre-adipocytes transfected with the respective Pre-miRTM miRNA Precursors. *Vegf* transcript levels showed a slight, but significant decrease ($P = 0.03$) in cells transfected with miR-378. There were no significant *Vegf* transcript level changes in cells transfected with miR-103, miR-107, miR-182 or miR-183 (**Figure 10A**). Immunoblot results revealed that p-S6k1/S6k1 ratio decreased in cells transfected with miR-183 by 34 % and miR-378 by 33 %. No changes in p-S6k1/S6k1 ratio were observed in cells transfected with

miR-103, miR-107 or miR-182 (**Figure 10B and C**). Both, altered Tsc1 protein levels and S6k1 phosphorylation as well as miR-378-mediated changes in *Vegf* gene expression suggest an attenuating effect of the miRNAs miR-183 and miR-378 on mTOR signaling.

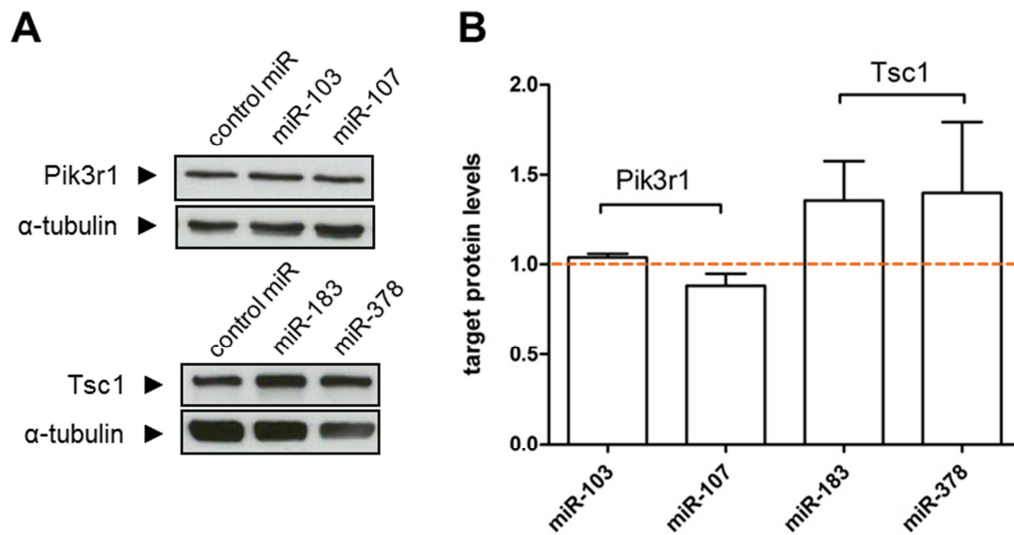


Figure 9: MiRNA-mediated effects on target protein levels

(A) Immunoblots of Pik3r1 protein in 3T3-L1 cells transfected with Pre-miRTM miRNA Precursor miR-103 and -107 and Tsc1 protein levels in cells transfected with miR-183 and -378 72 hours *post* transfection. α-tubulin was used as loading control. **(B)** Densitometric analysis of immunoblots from 2 independent experiments, each presented as relative ratio of the respective protein levels to α-tubulin. The dotted red line corresponds to control levels normalized to 1.0.

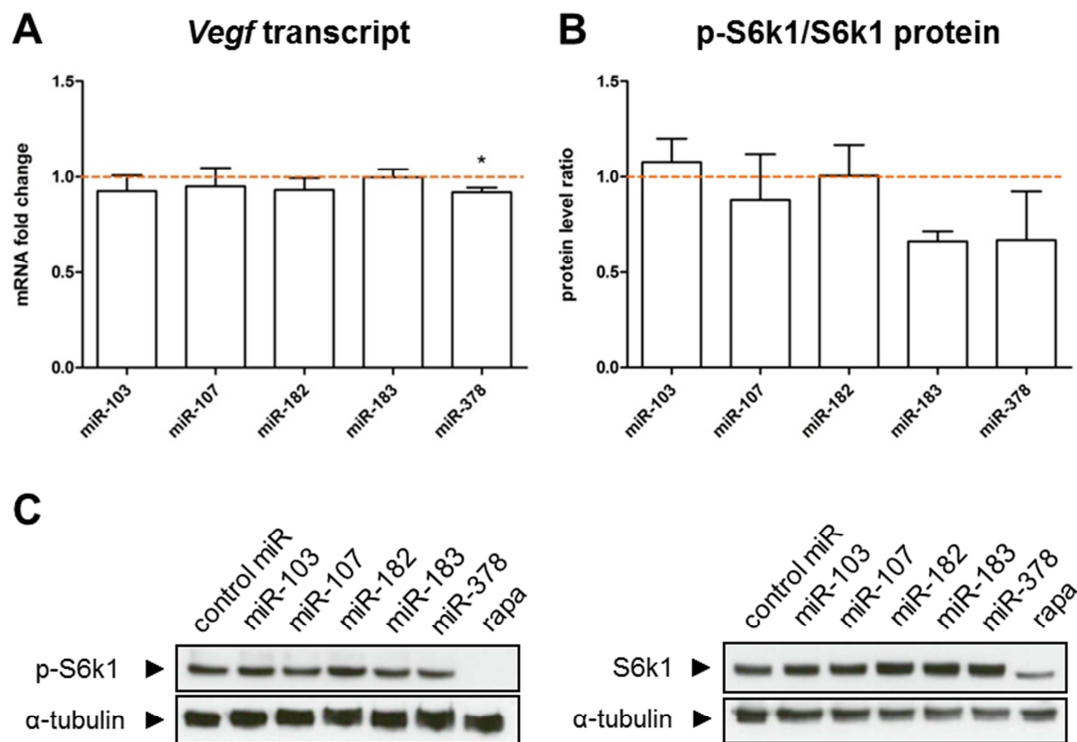


Figure 10: miRNA-mediated regulation of mTOR effectors

3 days after transfection of 3T3-L1 pre-adipocytes with the respective Pre-miRTM miRNA Precursor and control molecules. **(A)** *Vegf* transcript levels were quantified using rt-PCR. Mean values \pm S.E.M. of 5 independent experiments each performed in 6 pooled replicates and measured in technical triplicates. **(B)** P-S6K1 and S6K1 levels were quantified using immunoblotting. Densitometric analysis of immunoblots each presented as relative ratio of the respective protein levels to α -tubulin compared to control cells. Mean values \pm S.E.M. of 2 independent experiments. The dotted red line corresponds to control levels set to 1.0. **(C)** Immunoblots of p-S6K1 and S6K1 proteins. α -tubulin was used as loading control. Samples of rapamycin-mediated mTOR inhibition were included as positive control. A representative experiment is shown. * $P \leq 0.05$

5. MiRNA-mediated effects on adipocyte differentiation

To investigate putative effects of the candidate miRNAs during adipocyte differentiation, 3T3-L1 pre-adipocytes were transfected with the respective Pre-miRTM miRNA Precursors or Anti-miRTM miRNA Inhibitors. 48 hours *post* transfection induction of differentiation was initiated (day 0). Our primary hypothesis was that miR-183 and miR-378 are down-regulating *Tsc1* and thereby promote mTOR signaling. Therefore cells

were transfected with Anti-miRTM miRNA Inhibitors of miR-183 and miR-378 aiming for inhibition of adipogenesis. Intracellular miRNA levels at day 0, day 3 and day 6 of differentiation were assessed by rt-PCR (**Figure 11A**). MiR-183 and miR-378 levels were strongly down-regulated by 63 % ($P = 0.0001$) and by 52 % ($P = 0.031$) at day 0 of differentiation. Intracellular levels of miR-103, miR-107 and miR-182 showed a highly significant increase in cells transfected with the respective Pre-miRTM miRNA Precursors (**Figure 11B**) that persisted to day 6 post induction of differentiation.

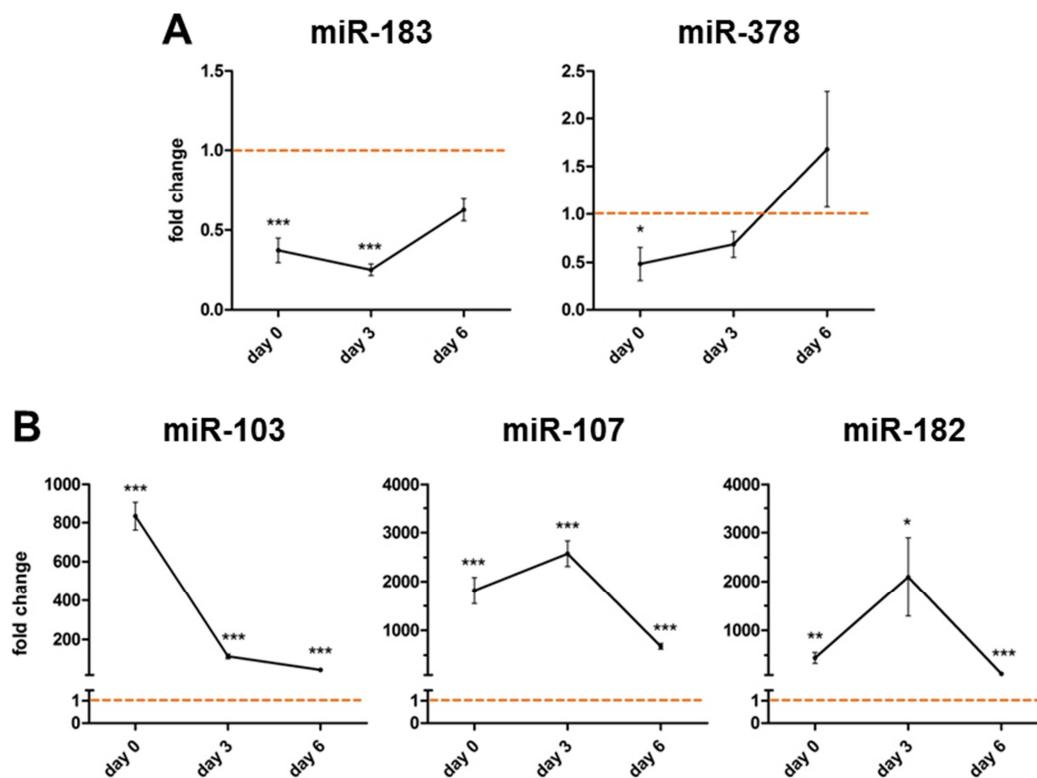


Figure 11: Time-course of miRNA levels during 3T3-L1 adipogenic differentiation after transfection with miRNA inhibitors or precursors

MiRNA levels were quantified using rt-PCR at day 0, day 3 and day 6 of 3T3-L1 differentiation. **(A)** miR-183 and miR-378 levels in cells transfected with the respective Anti-miRTM miRNA Inhibitor molecules at day -2. **(B)** miR-103, miR-107 and miR-182 levels in cells transfected with the respective Pre-miRTM miRNA Precursor molecules at day -2. Mean values \pm S.E.M. of 2 independent experiments each measured in technical triplicates. The dotted red line corresponds to the respective miRNA levels in control cells normalized to 1.0. * $P \leq 0.05$, ** $P \leq 0.01$, *** $P \leq 0.001$

Next, the relationship between miRNA changes and candidate target transcript levels during the time course of differentiation in transfected 3T3-L1 adipocytes were analyzed. *Tsc1* expression was altered in cells transfected with miR-183 and miR-378. However, *Pik3r1* and *Pik3r3* transcript levels did not show any alterations in cells transfected with miR-103, miR-107 or miR-182 (**Figure S 6**). To uncover miRNA-mediated effects on adipocyte differentiation adipocyte marker gene *Ppar γ* levels and pre-adipocyte marker gene *Dlk1* expression levels were determined at day 6 of differentiation. Marker transcript levels did not change in cells transfected with miR-103, miR-107 or miR-182 (data not shown), whereas *Ppar γ* was up-regulated by 39 % and *Dlk1* down-regulated by 42 % in cells transfected with anti-miR-183. Similar effects (*Ppar γ* up-regulation and *Dlk1* down-regulation) were shown for anti-miR-378 transfected cells. For these, expression level changes were highly significant in all experiments (**Figure 12**).

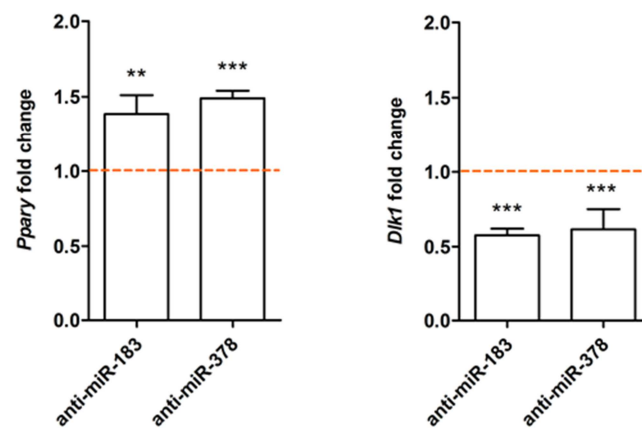


Figure 12: MiRNA-dependent influence on adipocyte and pre-adipocyte marker transcript levels

Quantification of adipocyte marker *Ppar γ* and pre-adipocyte marker *Dlk1* gene expression in cells differentiated for 6 days after transfection with the respective Anti-miRTM miRNA Inhibitors. Data of 2 independent experiments each performed in technical triplicates are given. Expression level changes were highly significant in all experiments. Mean values \pm S.E.M. The dotted red line corresponds to the respective mRNA levels in control cells normalized to 1.0. ** $P \leq 0.01$, *** $P \leq 0.001$

As a major characteristic of mature adipocytes, lipid droplet deposition was evaluated using two different lipid-droplet quantification methods. Cells were stained with lipid-

specific Oil Red O. An absorbance based quantification method determined the Oil Red O content in the supernatant of de-stained cells. This approach revealed that the miRNAs miR-103, miR-107 and miR-182 decreased lipid droplet deposition, while miR-183 and miR-378 had no influence (**Figure 13A**). Digital image analysis-based method additionally evaluated number and size of Oil Red O stained droplets by microscopy. This method revealed that the Oil Red O decrease in cells transfected with miR-107 or miR-182 was due to a reduced average lipid droplet size whereas the number of droplets did not change significantly. Reducing effects of miR-103 were not confirmed with this approach, since neither size nor number of lipid droplets reached statistical significance. The digital image-based approach further confirmed that anti-miR-183 and anti-miR-378 transfection did not influence lipid droplet size or numbers (**Figure 13B and C**).

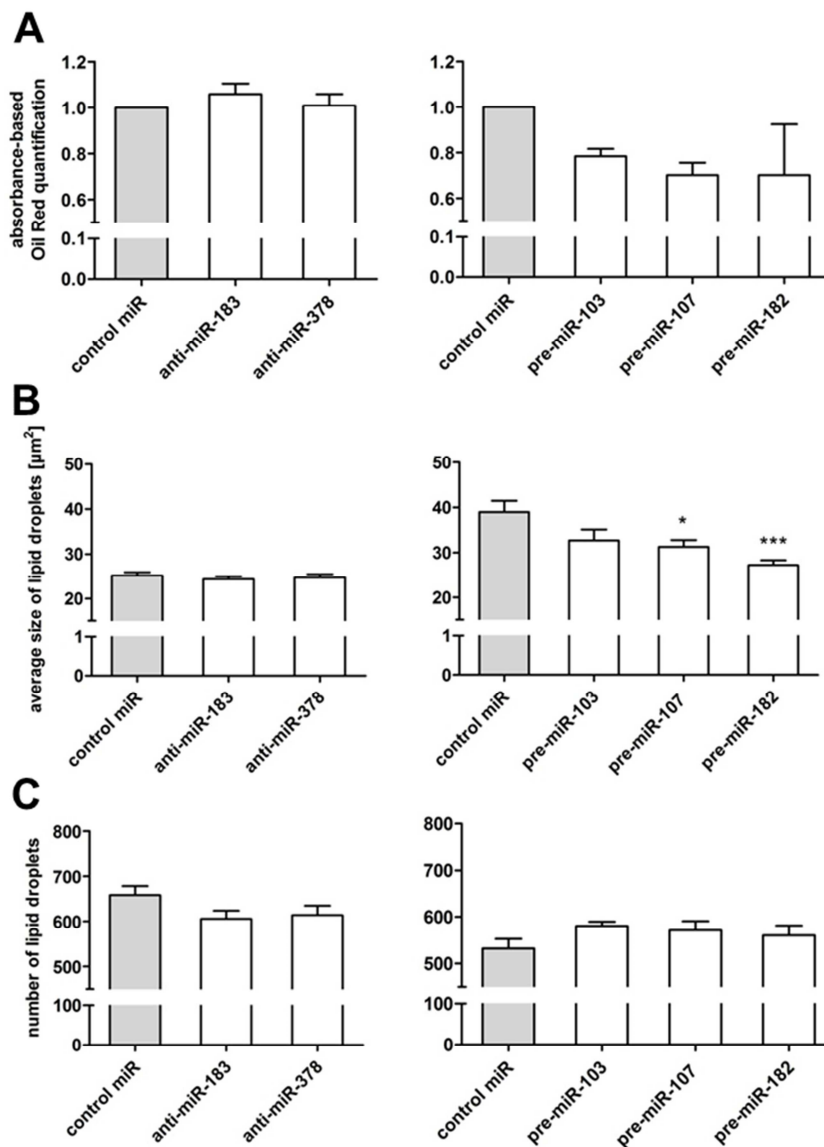


Figure 13: MiRNA-dependent decrease in lipid droplet deposition and size during adipocyte differentiation

Oil Red O quantification in 3T3-L1 adipocytes undergoing a differentiation protocol for 6 days after transfection of the respective Pre-miRTM miRNA Precursors or Anti-miRTM miRNA Inhibitors. **(A)** Absorbance-based method. 2 independent experiments each performed in technical duplicates. Mean values \pm S.E.M. **(B)** Average size and **(C)** number of lipid droplets per field of view quantified by digital image analysis. Data represent 2 independent experiments with 10 microscopy pictures each. Mean values \pm S.E.M. * $P \leq 0.05$, *** $P \leq 0.001$

6. Candidate targets for miRNA effects upstream Tsc1

Although miR-183 and -378 down-regulated *Tsc1* transcript levels, they surprisingly raised *Tsc1* on protein levels in 3T3-L1 cells. This phenomenon might be explained by functionally overruling regulation of targets upstream from *Tsc1*. According to our target prediction results (**Table S 1**), miR-378 could also target *Akt1* and miR-183 *Rsk3* protein (encoded by *Rps6ka2* gene). Both proteins are direct inhibitors of the Tsc complex (**Figure 5**) and thus could overrule miR-183 and -378 mediated *Tsc* down-regulation. To investigate miR-183 - *Rsk3* and miR-378 - *Akt1* target pairs, *Rps6ka2* and *Akt1* transcript as well as protein levels were determined in cells transfected with Pre-miRTM miRNA Precursors miR-183 and miR-378. However, miRNA-mediated down-regulation was neither observed on target transcript nor protein levels (**Figure 14**).

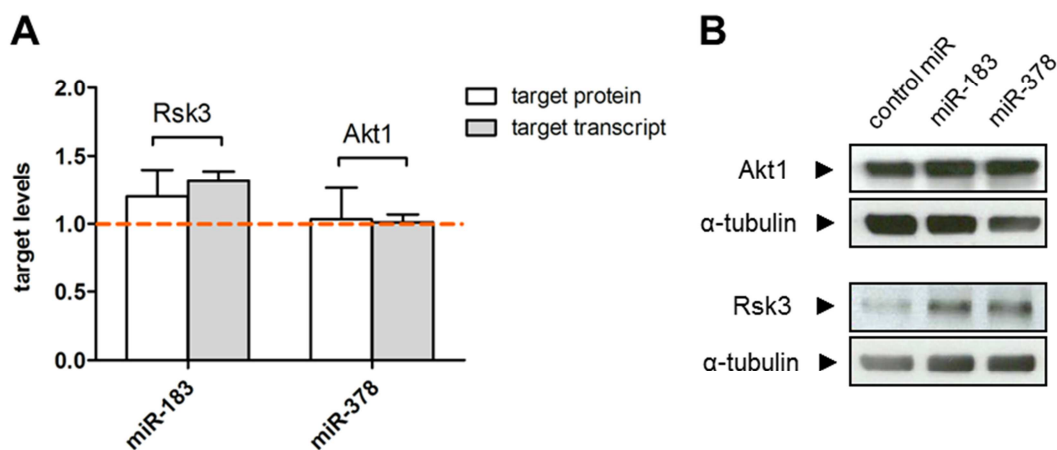


Figure 14: Effects of miR-183 and miR-378 on their predicted targets Rsk3 and Akt1

Protein and transcript levels were assessed 3 days after transfection of 3T3-L1 pre-adipocytes with the respective Pre-miRTM miRNA Precursor and Control molecules. **(A)** *Rps6ka2* (encoding for *Rsk3* protein) and *Akt1* transcript levels were quantified using rt-PCR. *Rsk3* and *Akt1* protein levels were quantified by immunoblotting. Densitometric analysis of immunoblots each presented as relative ratio of the respective protein levels to α -tubulin compared to control cells (dotted red line). Mean values \pm S.E.M. of 3 independent experiments. **(B)** Immunoblots of *Rsk3* and *Akt1* proteins. α -tubulin was used as loading control. A representative experiment is shown.

7. Evaluation of miRNA families and clusters on adipocyte differentiation

Particular attention was paid to the miRNA candidates miR-103 and -107 as well as miR-183 and -182, since these miRNAs hold special genetic backgrounds. The candidate miRNAs miR-103 and -107 form a miRNA family as their genes are paralogues deriving from gene duplication³³.

Firstly, the hypothesis of a miRNA family multiplying the effect of the single miRNA family members was investigated. Therefore 3T3-L1 pre-adipocytes were co-transfected with Pre-miRTM miRNA Precursors miR-103 and miR-107 and lipid droplet deposition as well as adipocyte marker gene levels were evaluated during adipocyte differentiation. Overall miRNA concentration utilized for transfection was equal to that used for cells transfected with a single miRNA, i.e. half of the concentration of each miRNA compared to single miRNA transfection was employed. Transfection efficiency was assessed by rt-PCR quantification of intracellular miRNA levels revealing very high relative increases at day 0 with persistent up-regulation up to day 6 (**Figure 15**).

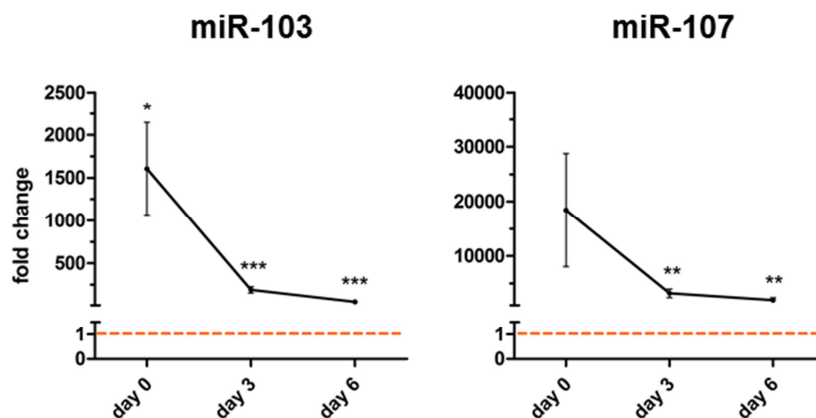


Figure 15: MiRNA expression during 3T3-L1 adipogenic differentiation after transfection with miRNA family 103/107 at day -2

MiR-103 and miR-107 levels were quantified using rt-PCR at day 0, day 3 and day 6 of 3T3-L1 differentiation after co-transfection at day -2. Mean values \pm S.E.M. of 2 independent experiments each measured in technical triplicates. The dotted red line corresponds to the respective miRNA levels in control cells normalized to 1.0.

* $P \leq 0.05$, ** $P \leq 0.01$, *** $P \leq 0.001$

To uncover effects of miRNA family 103/107 on adipocyte differentiation, lipid droplet deposition as well as adipocyte and pre-adipocyte marker expression levels were

determined at day 6 of differentiation. Lipid droplet deposition was evaluated using digital image analysis-based Oil Red O quantification. **Figure 16** shows that cells transfected with both, miR-103 and miR-107 gained significantly less lipid droplets during differentiation than cells transfected with each miRNA separately. Total area fraction of lipid droplets was reduced by 25 % ($P = 0.0012$) after family 103/107 transfection, whereas it slightly decreased by 11 % in cells transfected with miR-107 only and not altered after transfection of miR-103 only. The alterations in droplet area of cells transfected with miRNA family 103/107 were due to a significant decrease in lipid droplet number by 12 % ($P = 0.027$). In contrast, miR-107 alone decreased lipid droplets by reducing their size by 20 % ($P = 0.024$; **Figure 16**). Additionally adipocyte marker *Ppar γ* as well as pre-adipocyte marker *Dlk1* transcript levels were determined via rt-PCR. Gene expression of both markers were unaffected by transfection of miRNA family 103/107 (data not shown).

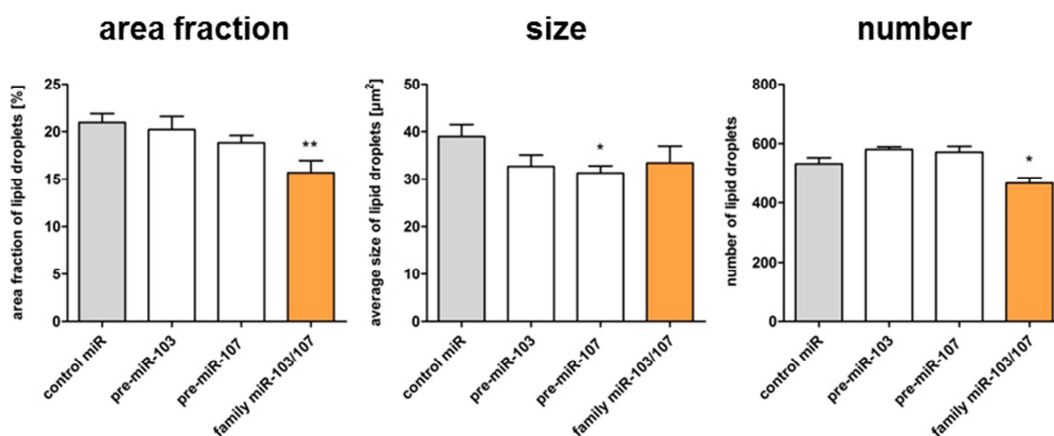


Figure 16: Effect of miRNA family miR-103/107 on lipid droplet deposition

Oil Red O quantification of 3T3-L1 cells undergoing the adipogenic differentiation protocol for 6 days after transfection of the respective Pre-miRTM miRNA Precursors. Area fraction, average size and number of lipid droplets per visual sight quantified by digital image analysis. 2 independent experiments with 10 microscopy pictures each were analyzed. Mean values \pm S.E.M. * $P \leq 0.05$, ** $P \leq 0.01$

The genes of the candidate miRNAs miR-182 and -183 are clustered together with miR-96 gene, meaning that their chromosomal distance is less than 10,000 nucleotides^{28, 32}. The hypothesis of miRNA cluster 183/96/182 multiplying the effect of the single miRNA

cluster members was investigated. Therefore 3T3-L1 pre-adipocytes were co-transfected with Pre-miRTM miRNA Precursors cluster members miR-182, miR-96 and miR-183. Overall concentration of miRNAs transfected was equal to that of cells transfected with a single miRNA (each one third of the concentration of single miRNA experiments). Transfection efficiency was assessed by quantification of intracellular miRNA levels (**Figure 17**).

After co-transfection with miR-183/96/182 cluster members, adipocyte and pre-adipocyte marker transcript levels (**Figure 18**) as well as lipid droplet deposition were determined. Adipocyte marker gene *Ppar γ* expression decreased by 18 %, whereas it did not change significantly in cells transfected with miR-182 or miR-96 separately. Pre-adipocyte marker *Dlk1* expression did not change in cells transfected with miRNA cluster 183/96/182. Likewise, lipid droplet deposition was not altered in cells transfected with miRNA cluster 183/96/182 (data not shown).

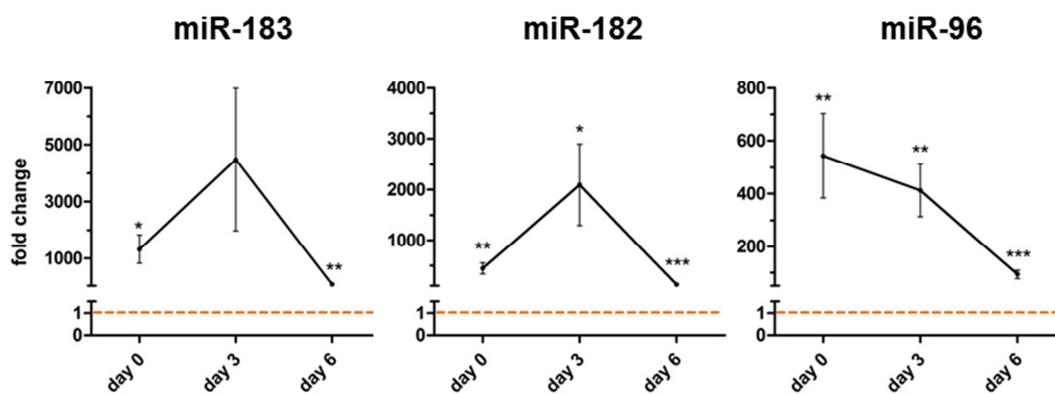


Figure 17: MiRNA expression during 3T3-L1 adipogenic differentiation after transfection with miRNA cluster 183/96/182 at day -2

MiR-183, miR-182 and miR-96 levels were quantified using rt-PCR at day 0, day 3 and day 6 of 3T3-L1 differentiation after co-transfection at day -2. Mean values \pm S.E.M. of 2 independent experiments each measured in technical triplicates. The dotted red line corresponds to the respective miRNA levels in control cells normalized to 1.0.

* $P \leq 0.05$, ** $P \leq 0.01$, *** $P \leq 0.001$

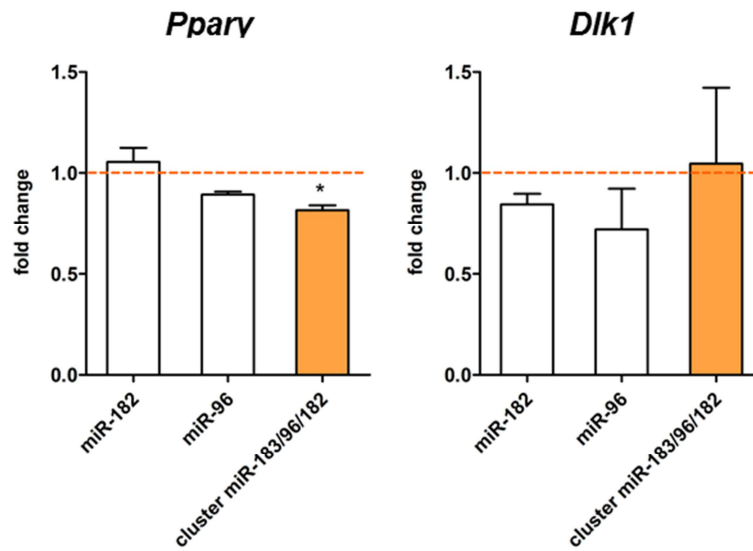


Figure 18: Effect of miRNA cluster 183/96/182 on adipocyte differentiation marker

Rt-PCR mediated quantification of adipocyte marker *Pparγ* and pre-adipocyte marker *Dlk1* gene expression in cells differentiated for 6 days after transfection with the respective Pre-miRTM miRNA Precursors. 2 independent experiments each performed in technical triplicates. The dotted red line corresponds to the respective mRNA levels in control cells normalized to 1.0. Mean values \pm S.E.M. * $P \leq 0.05$

D Discussion

MiRNAs have been reported to play a regulatory role in adipocyte differentiation, obesity and its associated pathologies^{34, 40, 49}. Among various nutrient signaling pathways regulating cell growth and cell differentiation towards maintenance of whole-body metabolic homeostasis, the mTOR pathway is an evolutionary conserved and well-studied regulator of adipogenesis⁸. The identification of miRNAs that influence adipocyte differentiation *via* mTOR nutrient signaling may provide a new approach for treatment or early diagnosis of chronic metabolic diseases. Four miRNAs have previously been implicated in mTOR nutrient signaling in the context of cancer and dermal wound healing³⁵⁻³⁸ but the pattern of miRNA regulation involved in mTOR signaling during adipocyte differentiation has not yet been elucidated. Thus we specifically aimed at identifying miRNAs that are influencing adipogenesis *via* targets in the mTOR pathway.

1. Rapamycin alters expression of miRNAs

In previous work of our group a set of mTOR associated miRNAs was already identified by differentiating adipocytes in the presence and absence of mTOR inhibitor rapamycin. 40 miRNAs showed differential regulation during adipocyte differentiation in the absence of any pharmacological alteration of the mTOR pathway. These results were consistent with earlier published studies reporting more than 30 of these differentially regulated miRNAs, that appear to be involved in regulating fat cell differentiation in adipocyte cell lines derived from humans and mice (reviewed in^{34, 40, 50}). Beyond this prior knowledge, our study additionally revealed differential regulation of miR-34a, -96, -106b, -148b, -678, -690 and -214*, all of these not yet documented in the context of fat cell differentiation. Some of these miRNAs have been implicated in insulin signaling or glucose metabolism, such as miR-96 or miR-690^{51, 52} or in cell cycle regulation, such as miR-96, miR-106b or miR-34a⁵³⁻⁵⁸. MiRNAs, whose expression is significantly altered during differentiation, must be expected to arise as a consequence of regulatory events occurring in numerous pathways that govern adipogenesis⁵⁹. To identify differentiation-associated miRNAs which are involved in mTOR signaling, one of the key nutrient sensing pathways, 3T3-L1 adipocytes were chronically treated with the mTOR-inhibitor rapamycin during differentiation procedure. Firstly, we confirmed the inhibitory effect of rapamycin on adipocyte differentiation as evidenced by quantification of marker transcripts and decreased deposition of lipid droplets^{15, 60, 61}. Thereafter, miRNA profiles

from 3T3-L1 cells undergoing an adipogenic differentiation protocol over eight days in the presence and in the absence of rapamycin were compared. Almost half of the miRNAs differentially regulated during adipogenesis were also sensitive to rapamycin-treatment. Chronic mTOR inhibition resulted in attenuation of regulation of these differentiation-associated miRNAs and corroborates the central role of mTOR in nutrient driven adipocyte differentiation. Four additional miRNAs were identified as 'rapamycin-sensitive', though showing no differential regulation during adipogenesis. These miRNAs may mediate differentiation-independent effects of mTOR signaling.

2. Selected miRNAs target predicted genes

2.1 *In silico* target prediction

The specific aim of this study was to discover the targets of mTOR associated miRNAs to unravel their regulatory function within mTOR signaling. To identify presumptive direct miRNA-target pairs within the mTOR pathway, our set of 'rapamycin-sensitive' miRNAs was subjected to a stringent *in silico* target prediction. This is an important step for high-throughput pre-selection of putative targets, to narrow down the number of miRNA-target pairs which have to be functionally confirmed in the next steps.

Computational miRNA target prediction still remains challenging as the binding of miRNAs to their respective target genes does not require full complementarity and the binding patterns are not yet fully understood⁶². Various prediction tools have been developed based firstly on the complementarity between the 5' seed region of the miRNA and the 3'UTR of the target gene, secondly on thermodynamic stability of miRNA-target alignments and thirdly on miRNA:mRNA duplex conservation between species⁶³. Since each prediction tool applies distinct algorithms, they predict differing sets of targets. Furthermore, it has already been reported that target predictions may generate an estimated rate of 31 % false positive targets⁶⁴. To overcome these limitations we aimed to increase the prediction specificity by combining five different prediction algorithms. The set of 'rapamycin-sensitive' miRNAs was subjected to PITA, miRanda, targetScanS, pictar and targetspy algorithms and only those miRNA-target pairs with a consensus target prediction of at least 2 algorithms were considered as presumptive candidates. Although this stringent approach may lead to higher specificity (percentage of correctly predicted among overall predicted ones), it may result in decreased sensitivity (percentage of correctly predicted targets out of total correct ones)⁶². This may lead to the loss of some miRNA-target pairs in our approach.

However, subjecting the ‘rapamycin-sensitive’ miRNAs to our stringent prediction approach revealed that more than two thirds of these miRNAs were indeed predicted to target genes of the mTOR pathway. This finding indirectly confirmed the utility of rapamycin in the experimental discovery approach. For functional confirmation we selected five miRNA-target pairs according to the *in silico* prediction results: miR-183-*Tsc1*, miR-378-*Tsc1*, miR-103-*Pik3r1*, miR-107-*Pik3r1* and miR-182-*Pik3r3*. All of these miRNAs already showed strong rapamycin effects in the differentiation experiments and were predicted to target central genes of the mTOR pathway.

To validate the set of ‘rapamycin-sensitive’ miRNAs in reverse, the computational pathway-prediction tool DIANA-miRPath was used. This tool is focused on the identification of miRNA targeted pathways and thus provides an insight into functional characterization of the predicted miRNA target genes⁶⁵. With this method, we investigated the molecular pathways which may be altered by the set of rapamycin-sensitive miRNAs. Here, mTOR pathway targets were found to be significantly enriched in the set of predicted rapamycin-sensitive miRNA targets. These results are in line with the findings of *in silico* target prediction and they additionally confirm our experimental discovery approach.

2.2 Functional confirmation by luciferase-based reporter assays

In a first step, functional confirmation of miRNA targets was investigated by luciferase-based reporter assays, a routinely used and efficient assay for the validation of individual miRNA-mRNA interactions. For this purpose, HEK-293 cells were co-transfected with the respective miRNA molecules and reporter plasmids harboring the 3’UTRs of the respective, predicted miRNA target genes.

Reporter assays revealed that miR-183 and miR-378 bind to the 3’UTR of their predicted target gene *Tsc1* and that miR-103 binds to its target gene *Pik3r1*. However, physical interaction of miR-107 with *Pik3r1* 3’UTR and miR-182 with *Pik3r3* 3’UTR was not confirmed. Herewith we show that miR-183, miR-378 and miR-103 may target components of mTOR signaling, which needs to be further confirmed in a second, functional approach. The rate of interactions we detected is concordant with Lewis *et al.* reporting an estimated false positive *in silico* prediction rate as high as one third⁶⁴. Nevertheless, all five miRNA-mRNA target pairs were subjected to further functional confirmation assays.

2.3 Functional confirmation by transfection experiments

As a second approach for functional confirmation of the miRNA-target pairs, miRNA-mediated effects on target gene expression were investigated. Therefore adipocytes were transfected with the respective miRNAs and target transcript levels were quantified.

To identify ideal concentrations of miRNA that are transfected and appropriate time points for cell harvest, some pre-experiments were performed. Transfection efficiencies were evaluated by determination of intracellular miRNA levels *via* rt-PCR and by measuring the percentage of transfected cells *via* flow cytometry. On the one hand the flow cytometry-based approach for establishment of transfection conditions is very fast, simple in workflow and enables simultaneous determination of cell viability. On the other hand this approach investigates conditions in cells transfected with a labelled control siRNA and thus is not specific for individual miRNAs. We thus additionally confirmed flow cytometry results *via* a rt-PCR-based approach. Although rt-PCR is more time-consuming, this approach enables to investigate fold changes of individual miRNAs and thus is essential to validate successful transfection in the experiment.

For both approaches cells were transfected with various concentrations of siRNA/miRNA and harvested at various time points. Flow cytometry results of siRNA transfected cells as well as rt-PCR results of cells transfected with the respective candidate miRNAs were concordant: Transfection efficiency increased with increasing concentrations of transfected miRNA molecules and decreased with time. Since a longer time span *post* transfection allows the cell to process miRNA-mediated effects on target transcripts and to retain a high number of viable cells, transfection was carried out with 20 pmol of the respective miRNAs and cells were harvested 72 hours *post* transfection for further validation experiments. These pre-experiments showed that the flow-cytometry based approach is suitable for fast screening of many different experimental conditions of transfection, whereas rt-PCR based validation of successful transfection is mandatory to control intracellular levels of the individual miRNAs. We thus validated successful transfection in our experiments *via* quantification of the respective intracellular miRNA levels and noticed that the relative increase is miRNA dependent. This may be due to individual endogenous expression levels of the respective miRNAs. MiR-107 for example showed lower endogenous expression ($C_T = 34.5 \pm 0.3$) and consequently higher fold changes (~7,400), whereas miR-182 is

higher expressed under physiological conditions ($C_T = 28.6 \pm 0.4$) and increases 923-fold after transfection.

With this knowledge, miRNA-mediated effects on target transcript levels were investigated for further functional confirmation in transfection experiments. For this purpose, target gene expression changes were quantified in adipocytes transfected with the respective miRNAs. These experiments revealed that miR-183 and miR-378 down-regulated *Tsc1* gene expression and miR-103 down-regulated *Pik3r1* expression, whereas miR-107 did not change its predicted target transcript *Pik3r1* levels and miR-182 did not change *Pik3r3* transcript levels. These results resemble those of luciferase-based reporter assays. However, a limitation of these experiments is that miRNA transfection results in supra-physiological miRNA levels, which may lead to multiple artifacts⁶⁶. Another drawback for validation of miRNA-target pairs with this method is that transcriptomes highly depend on cell type, culture conditions etc.⁶². That is why our experiments were performed using adipocytes in an environment of nutrient satisfaction, where mTOR signaling should be activated and hence even lower gene expression changes are detectable. Additionally, the miRNA-transfection approach can not distinguish direct from indirect targets, a disadvantage we overcome by combination with reporter assay results, which are indicating direct miRNA effects⁶². To eliminate effects on cells and gene expression mediated by the transfection procedure, we used cells transfected with a control miRNA for normalization. These findings, together with the results from luciferase-based reporter assays indicate that miR-183, miR-378 and miR-103 may target genes within mTOR signaling, which needs to be further confirmed on protein level.

2.4 Functional confirmation on protein level

Thus, in the next step candidate miRNA-mediated effects on mTOR targets were investigated on protein level. Therefore protein level changes were quantified in adipocytes transfected with the respective miRNAs.

Immunoblotting of miR-103 and miR-107-transfected cells revealed that there were no detectable changes in *Pik3r1* protein levels. The result for miR-107-transfected cells is not surprising as miR-107 did neither change *Pik3r1* transcript levels nor luciferase activity in reporter assays. In contrast, *Pik3r1* protein levels remained unaffected in miR-103 transfected cells, although miR-103 has been shown to down-regulate *Pik3r1* gene expression in the above experiments. Although immunoblotting is considered as a rather qualitative method to detect a protein in a complex sample, improvements in

terms of sensitivity and stability of the detection signal allow its use for relative quantification. However, due to limitations resulting from a narrow detection range, difficulties to determine linear quantification ranges for each protein and variance arising from sample loading, protein transfer and signal imaging, the detection of small alterations in protein levels *via* immunoblotting still remains challenging^{67, 68}. Thus either the miR-103-mediated effect on its target gene is not powerful enough to be functionally relevant on protein level or the alteration in protein expression is not strong enough to be detected by semi-quantitative immunoblotting. Moreover, as described for the transcriptome, also the proteome is highly dependent on cell physiology, so that miRNA-independent regulation mechanisms may overrule miRNA-mediated protein down-regulation⁶². For elimination of putative cell physiological effects, all cells were cultured under equal conditions of an environment of nutrient satisfaction, where mTOR signaling is activated and hence gene expression changes detectable, as for transfection experiments. A putative effect of miR-103 as well as of miR-107 on mTOR signaling (possibly *via* so far uninvestigated targets) was examined in subsequent experiments.

MiR-183 and miR-378 transfection resulted in a slight Tsc1 protein up-regulation, even though both miRNAs have been shown to decrease *Tsc1* on transcript level. The unexpected phenomenon of inversely correlated Tsc1 transcript and protein levels could be due to functionally overruling regulation of up-stream targets resulting in deregulated protein levels in the downstream signaling cascade. To further investigate this hypothesis, we returned to *in silico* target prediction. MiR-183 was additionally predicted to target *Rps6ka2* gene encoding Rsk3 protein and miR-378 was predicted to target Akt1, both up-stream inhibitors of the Tsc complex. Overruling down-regulation of up-stream inhibitors could explain the observed Tsc1 protein increase. Thus we determined Rsk3 and Akt1 transcript and protein levels in 3T3-L1 cells transfected with miR-183 and miR-378 respectively. However, results showed that neither miR-183 nor miR-378 down-regulated the predicted targets.

Table 6 provides an overview of miRNA-mediated effects on predicted targets, mTOR signaling and adipocyte differentiation.

Table 6: Summary of miRNA effects on predicted targets, mTOR signaling and adipocyte differentiation

Effects which would lead to attenuation of adipocyte differentiation are highlighted in green, effects which would drive adipocyte differentiation are highlighted in red. *, ** and *** indicate significant changes; ND: protein levels were not determined.

	<i>miR-183</i>	<i>miR-378</i>	<i>miR-103</i>	<i>miR-107</i>	<i>miR-182</i>
binding to target 3'UTR	***	**	**		
regulating target gene	**	***	***		
regulating target protein					ND
influencing mTOR output					
influencing differentiation	** 1)	*** 1)		*2)	*** 2)

1) alterations in adipocyte and pre-adipocyte marker genes 2) alterations in lipid droplet deposition

3. Effects of selected miRNAs on mTOR-signaling

To further investigate the candidate miRNA effects on mTOR signaling, adipocytes were transfected with the respective miRNA molecules. Since mTORC1 promotes angiogenesis *via Vegf* gene expression stimulation and regulates protein synthesis *via* S6k1 phosphorylation, miRNA effects on mTOR signaling were evaluated by determination of p-S6k1/S6k1 ratio and *Vegf* transcript levels.

Since miR-182, miR-103 and miR-107 were not confirmed to influence their target gene and/or protein levels in the previously described experiments, it was not surprising that they did not influence mTOR signaling during differentiation (**Table 6**). This would lead to the conclusion that these miRNAs do not influence mTOR signaling up-stream the investigated effectors. But since these miRNAs showed rapamycin-sensitive expression changes, miR-103 and miR-107 might still target *Eif4b*, another predicted gene downstream of mTOR complex 1 and the investigated effectors. Mir-182 might be involved in autophagy, a pathway which can be activated by mTOR signaling *via* the predicted target and mTOR effector *Ulk*.

In contrast to miR-103, -107 and -182, transfection of miR-183 and miR-378 decreased S6k1 phosphorylation though not reaching statistical significance. This result is in concordance with the previous experiment, in which miR-183 and miR-378 transfection resulted in increased mTOR inhibitor Tsc1 protein levels (**Table 6**) and may point to an effect of these miRNAs on general protein synthesis. MiR-378 additionally decreased Vegf transcript levels significantly and thus this miRNA might affect angiogenesis as well as general protein synthesis. These findings indicate that miR-183 and miR-378 indeed influence mTOR nutrient signaling and thereby expand the list of the four previously experimentally confirmed miRNAs that target the mTOR pathway in other biological settings, namely miR-99a and -b, miR-100 and miR-199a-3p³⁵⁻³⁸.

4. Effects of selected miRNAs on adipocyte differentiation

To investigate the candidate miRNA effects on adipocyte differentiation, adipocytes were transfected with the respective miRNAs/anti-miRNAs and subsequently differentiation was initiated. After 6 days of differentiation lipid droplet deposition as well as adipocyte marker *Ppar γ* and pre-adipocyte marker *Dlk1* expression levels were quantified. *Ppar γ* is a transcription factor leading to fundamental changes in gene expression resulting in the stimulation of proteins critical for adipogenesis. Since *Ppar γ* expression is maintained throughout the differentiation process, *Ppar γ* transcript levels are routinely used as adipocyte marker. Although the mechanisms, by which *Dlk1* (alias pre-adipocyte factor-1) influences adipocyte differentiation are not as intensively studied as those of *Ppar γ* , it is a generally accepted pre-adipocyte marker.

Lipid droplets were visualized *via* Oil Red O staining and then quantified applying two different methods. The shorter approach for quantification was absorbance measurement of the supernatant from de-stained cells. Since the results are strongly depending on equal confluence of cells between wells, we normalized the values to cell numbers. In this study Oil Red O absorbance values were normalized to this parameter *via* Cellscreen microscopy. There are only few other techniques available to gain more information about lipid droplets, such as amount and size. Our approach for determination of lipid droplet size and numbers was to take digital microscopy pictures of Oil Red O stained cells, which are subsequently analyzed by a digital image analysis software⁴⁴. Since microscopy pictures are taken from areas with complete cell coverage, it is not necessary to determine cell numbers per well. One advantage of this method is that only a standard light microscope and the freely available software tool ImageJ is needed. ImageJ enables automating of the commands and thus reduces time

requirements. Further, because of the simplicity of this software tool, the approach is applicable for users without previous imaging or programming expertise. The most important advantage is the possibility to evaluate individual lipid droplet size and numbers, though a limiting factor can occur by incomplete droplet separation of highly dense packed droplet clusters. In our study, however, experiments revealed consistency between the microscopy-based and the absorbance-based method.

Digital microscopy picture analysis showed a significant decrease of lipid droplet deposition in cells transfected with miR-107 and miR-182. The absorbance-based method accordingly showed declining absorbance values normalized to cell coverage. Additionally, the microscopy-based method revealed that the decrease in lipid droplet formation is due to droplet size reduction. Thus these miRNAs seem to influence adipocyte differentiation by affecting lipid droplet size (**Table 6**). While the molecular mechanism are not yet fully understood, it is already known that S6k1, a down-stream effector of mTOR, controls lipid metabolism⁶⁹. Although miR-107 and miR-182 expression appeared to be highly sensitive to rapamycin treatment in our study, these miRNAs influenced lipid droplet formation S6k1 phosphorylation independently in our study. But there are S6k1-independent mechanisms of mTOR mediated *de novo* lipogenesis already known. Firstly, mTOR complex 1 can stimulate lipogenic genes by induction of the key transcription factor *Pparγ* via 4Ebp1⁶⁹. However, since the adipocyte marker gene *Pparγ* expression remained unchanged in cells which were differentiated after miR-107 and miR-182 transfection, these miRNAs may not influence lipid droplet deposition via this mTOR-4Ebp1-Pparγ axis. A second mechanism linking mTOR to lipid droplet formation is mTOR mediated inhibition of Atgl transcription (adipose triglyceride lipase), an enzyme which controls lipid homeostasis⁹. Thirdly it has been reported that mTOR complex 1 can promote *de novo* lipogenesis via Srebp-1 activation, a transcription factor controlling gene expression of lipogenic genes⁶⁹. Thus miR-182 and miR-107 may influence lipid droplet formation via targets down-stream of mTOR being part of this Atgl or Srebp-1 mediated mechanisms. Thus these miRNAs could show rapamycin-sensitivity on the one hand and pS6k1 and *Pparγ* independence on the other hand. Concordant to our results, miR-107 and miR-182 have been implicated in adipocyte differentiation in other studies^{34, 40}. Meng *et al.* showed that under hypoxic conditions miR-107 suppressed endothelial progenitor cell differentiation via Hif1β, whereas in our study miR-107 did not influence the mTOR-Hif1-Vegf angiogenesis pathway under physiological oxygen conditions⁷⁰. These findings demonstrate an example for a miRNA effect dependent on the respective physiological

conditions. To the best of our knowledge the targets by which miR-182 influences adipocyte differentiation have not yet been discovered.

Adipocytes transfected with miR-103 did not show any differences in absorbance-based or in microscopy-based Oil Red O quantification. Further, the expression of pre-adipocyte and adipocyte marker genes was not altered by miR-103 transfection (**Table 6**). Thus miR-103 did neither influence the mTOR effectors investigated nor differentiation markers or lipid droplet deposition in our study. These findings were consistent with an earlier study reporting normal triglyceride levels in differentiated 3T3-L1 adipocytes ectopically expressing miR-103, although the same study reported a miR-103-mediated increase in triglycerides in the early stage of 3T3-L1 differentiation⁷⁰. Reported *in vivo* studies are inconsistent: in mice mir-103 was found to be down-regulated in mature adipocytes, whereas it was up-regulated in human adipose tissue³⁴. Thus miR-103 may accelerate adipocyte differentiation while not affecting the final state of the differentiated cell.

Lipid droplet deposition remained unchanged in differentiated cells transfected with anti-miR-183 or anti-miR-378 in our study. However, both miRNAs showed an attenuating effect on adipocyte differentiation as anti-miR-183 and anti-miR-378 treatments led to increased adipocyte marker and decreased pre-adipocyte marker gene expression in our study (**Table 6**). Triacylglycerol molecules are neutral lipids synthesized by cells in times of nutrition excess and are stored in lipid droplets⁷¹. Thus synthesis of triacylglycerol may correlate with lipid droplet formation. In concordance to our results, another study inhibiting miR-378 *via* antagomirs discovered no significant changes in triacylglycerol levels or adipocyte morphology in the late stages of differentiation. However, the same study reported increased triacylglycerol levels and accelerated lipid droplet growth in early stages of differentiation after overexpression of miR-378 and miR-378*⁷². Although it was not possible to distinguish whether the effects on lipogenesis were due to miR-378 or miR-378* in that study, the authors stated that miR-378 together with miR-378* stimulate adipogenesis in the early stages of differentiation. Our study describes an attenuating effect of miR-378 in the late stages of differentiation: the opposite effect in the early stages of differentiation may either be caused by miR-378*, which is not investigated in our study, and/or miR-378 might be involved in a negative feedback regulatory mechanism in the late stages of differentiation. Targeting genes within this feedback mechanism may overrule less important targets, such as previously described for Tsc1 on protein level, thereby

leading to inversely correlated Tsc1 transcript and protein levels. Our results showed firstly that miR-378 was strongly up-regulated in the late phase of adipocyte differentiation (**Figure S 7**), secondly that miR-378 indirectly increased mTOR inhibitor Tsc1 and thirdly attenuated mTOR effectors. Taken together these findings are consistent with our hypothesis of miR-378 being involved in a negative feedback regulation of mTOR signaling. We propose that miR-378 might be involved in the well characterized suppression of Pi3k by mTORC1 activated S6k1^{73, 74}. In this process prolonged growth factor-mediated mTOR activation and hence S6k1 phosphorylation strongly down-regulate insulin signaling *via* the Pi3k-Tsc-mTOR axis. *In vivo* this mechanism of uncoupling Pi3k may be required to block further activation as soon as sufficient growth has been reached⁷³.

In our study miR-183 did not influence lipid droplet deposition, but revealed an attenuating effect on adipocyte differentiation as evidenced by its influence on adipocyte/pre-adipocyte marker gene expression at late stages of differentiation. These results are in line with the attenuating effect of this miRNA on mTOR effector S6k1 and the increasing effect on mTOR inhibitor Tsc1. Chen *et al.* could not detect a miR-183 dependent influence on marker gene expression changes in the late stages of differentiation, however, in the early stages of differentiation, they report a miR-183 dependent increase in marker gene expression and lipid droplet deposition⁷⁵. The effect of miR-183 on adipocyte differentiation seems to be opposed in early and late stages of differentiation as already described for miR-378. Besides miR-378, miR-183 was also strongly up-regulated in the late phase of adipocyte differentiation (**Figure S 7**) and affected genes of the Tsc-mTOR-S6k1 axis in an adipocyte differentiation attenuating manner. Thus miR-183 may also be part of a negative feedback mechanism, such as the S6k1 phosphorylation activated Pi3k suppression^{73, 74}. Such mechanism would lead to overruling effects on previously described miR-183 target Tsc1 on protein level as already mentioned for miR-378.

The better understanding of the involvement of miRNAs in adipocyte differentiation may give important inputs about the regulation of mammalian adipogenesis and might even provide an approach for therapeutic options. For example, recent studies detected miRNAs as biomarkers in several chronic diseases like cardiovascular disease, cancer and type 2 diabetes⁷⁶⁻⁷⁸. Thus, in the future, miRNAs might also be used for clinical diagnosis and treatment monitoring of chronic diseases³⁴.

5. MiRNA cluster 183/96/182 and miRNA family 103/107

Clustered miRNAs derive from a common multi-cistronic pri-miRNA and thus are influenced by similar regulation mechanisms^{28, 32}. That is why clustered miRNAs are thought to be functionally related and, like miRNA families, of particular biological relevance. MiRNA families derived from gene duplication thereby often share seed sequences³³. In contrast to miRNA clusters, miRNA families may act redundantly by targeting similar gene sets, whereas clustered miRNAs may act coordinately by targeting different genes within one pathway⁵¹. We thus investigated potential additional effects of clustered miRNAs or miRNA families compared to its individual miRNA members on adipocyte differentiation. For this purpose, 3T3-L1 pre-adipocytes were transfected with either miRNA cluster 183/96/182 or miRNA family 103/107 and subsequently subjected to differentiation.

We found that miRNA cluster 183/96/182 influences adipocyte differentiation by down-regulating adipocyte marker *Pparγ* gene expression, while miR-182 and miR-96 alone did not affect marker gene levels. However, miR-183 alone had a strong effect on *Pparγ* and *Dlk1* gene expression in the above experiments. The effects of the cluster may thus mainly be mediated by miR-183 in our study. However, cluster 183/96/182 has previously been described to play an important regulatory role by targeting several signaling pathways, including insulin signaling⁵¹. Since the expression of this cluster was characterized by high rapamycin-sensitivity, our study expands this knowledge by adding mTOR signaling as presumptive function of this cluster.

MiRNA family 103/107 influenced adipocyte differentiation by decreasing lipid droplet numbers, whereas miR-107 alone reduced lipid droplet size and miR-103 alone did not affect lipid droplet deposition at all. Although miR-103 and miR-107 reside on different chromosomes they are located within introns of a set of genes encoding for enzymes involved in fatty acid, amino acid, cholesterol, pyruvate or glucose metabolism⁷⁹. Wilfred *et al.* reported that bioinformatics predict target genes of these miRNAs in lipid metabolism, which could result in decreasing fatty acid synthesis and uptake. Until now, however, experimental data for this hypothesis was lacking⁷⁹. Our study may provide the first experimental evidence for the involvement of this miRNA family in lipid metabolism by decreasing lipid droplet deposition. This effect is likely mTOR-signaling associated due to the miRNAs' rapamycin-sensitive expression changes during adipocyte differentiation. We conclude from these findings, that miRNA families may

exhibit regulatory effects on adipogenesis additionally to those of the respective single miRNAs.

Our findings support a recently suggested concept of miRNA regulation: Entire networks of multiple miRNAs targeting multiple genes should be considered, instead of one miRNA-one target gene pairs^{31, 66}. On the one hand one gene may be targeted by multiple miRNAs, on the other hand one miRNA may target multiple genes even within one pathway, thereby reaching biological importance, despite weak effects of individual miRNA-target pairs. A more complete understanding of the complex regulatory networks of miRNAs and their targets still remains a challenge in the miRNA field that needs to be overcome^{31, 66}.

E Summary

Obesity is defined as abnormal or excessive fat accumulation which may have adverse effects on health. On adipose tissue level the development of obesity is dependent on the coordinated interplay of adipocyte hypertrophy, pre-adipocyte proliferation and differentiation of pre-adipocytes into mature fat cells. The mechanistic target of rapamycin (mTOR) signaling is an evolutionary conserved and well-studied nutrient-signaling pathway adapting cell differentiation to nutrient availability. In addition, miRNAs appear to play a crucial regulatory role as more than 40 miRNAs have previously been reported as being associated with adipocyte differentiation. In this study, we specifically aimed at identifying distinct miRNAs that are governing nutrient-driven adipogenesis *via* the mTOR pathway.

Taken together, we identified a subset of 16 miRNAs showing both responsiveness to rapamycin and prediction as targets within the mTOR pathway. We confirmed target 3'UTR binding and target transcript regulation of the predicted miRNA-target pairs miR-183 - *Tsc1*, miR-378 - *Tsc1* and miR-103 - *Pik3r1*. Unexpectedly *Pik3r1* protein levels were not altered and *Tsc1* protein levels were inversely correlated to *Tsc1* transcript levels. Nevertheless *Tsc1* protein up-regulation was consistent with an attenuating effect of miR-183 and miR-378 on mTOR signaling and adipocyte marker transcript levels. Since miRNA-mediated effects were detected during the late stages of differentiation, these miRNAs may be involved in negative feedback regulatory mechanisms. We found that miR-107 and miR-182 reduced lipid droplet size during adipocyte differentiation. The present study provides first experimental evidence for the predicted effects of miRNA family 103/107 on lipid metabolism. Moreover, our data are suggestive that miRNA families may exhibit further effects on adipogenesis additionally to those of the respective single miRNAs.

Especially the effect of miR-107, miR-182 and miRNA family 103/107 on adipocyte differentiation makes them promising targets for further investigation. Above all the attenuating effect of miR-183 and miR-378 on mTOR signaling as well as adipocyte differentiation may also suggest an utility of these miRNAs as biomarkers for nutrient-driven dysregulation of adipogenesis.

F References

1. Fact Sheet N°311 - Obesity and overweight. In.: World Health Organization; 2013.
2. Withrow D, Alter DA: The economic burden of obesity worldwide: a systematic review of the direct costs of obesity. *Obes Rev* 12, 131-141 (2011).
3. Jordan SD, Konner AC, Bruning JC: Sensing the fuels: glucose and lipid signaling in the CNS controlling energy homeostasis. *Cell Mol Life Sci* 67, 3255-3273 (2010).
4. Avram MM, Avram AS, James WD: Subcutaneous fat in normal and diseased states 3. Adipogenesis: from stem cell to fat cell. *J Am Acad Dermatol* 56, 472-492 (2007).
5. Gregoire FM, Smas CM, Sul HS: Understanding adipocyte differentiation. *Physiol Rev* 78, 783-809 (1998).
6. Gregoire FM: Adipocyte differentiation: from fibroblast to endocrine cell. *Exp Biol Med (Maywood)* 226, 997-1002 (2001).
7. Green H, Kehinde O: An established preadipose cell line and its differentiation in culture. II. Factors affecting the adipose conversion. *Cell* 5, 19-27 (1975).
8. Marshall S: Role of insulin, adipocyte hormones, and nutrient-sensing pathways in regulating fuel metabolism and energy homeostasis: a nutritional perspective of diabetes, obesity, and cancer. *Sci STKE* 2006, re7 (2006).
9. Chakrabarti P, English T, Shi J, Smas CM, Kandror KV: Mammalian target of rapamycin complex 1 suppresses lipolysis, stimulates lipogenesis, and promotes fat storage. *Diabetes* 59, 775-781 (2010).
10. Jewell JL, Guan KL: Nutrient signaling to mTOR and cell growth. *Trends Biochem Sci* 38, 233-242 (2013).
11. Laplante M, Sabatini DM: mTOR signaling in growth control and disease. *Cell* 149, 274-293 (2012).
12. Ma XM, Blenis J: Molecular mechanisms of mTOR-mediated translational control. *Nat Rev Mol Cell Biol* 10, 307-318 (2009).
13. Jiang BH, Liu LZ: PI3K/PTEN signaling in angiogenesis and tumorigenesis. *Adv Cancer Res* 102, 19-65 (2009).
14. Hudson CC, Liu M, Chiang GG, Otterness DM, Loomis DC, Kaper F, Giaccia AJ, Abraham RT: Regulation of hypoxia-inducible factor 1alpha expression and

- function by the mammalian target of rapamycin. *Mol Cell Biol* 22, 7004-7014 (2002).
15. Cho HJ, Park J, Lee HW, Lee YS, Kim JB: Regulation of adipocyte differentiation and insulin action with rapamycin. *Biochem Biophys Res Commun* 321, 942-948 (2004).
 16. Polak P, Cybulski N, Feige JN, Auwerx J, Ruegg MA, Hall MN: Adipose-specific knockout of raptor results in lean mice with enhanced mitochondrial respiration. *Cell Metab* 8, 399-410 (2008).
 17. Um SH, D'Alessio D, Thomas G: Nutrient overload, insulin resistance, and ribosomal protein S6 kinase 1, S6K1. *Cell Metab* 3, 393-402 (2006).
 18. Birse RT, Choi J, Reardon K, Rodriguez J, Graham S, Diop S, Ocorr K, Bodmer R, Oldham S: High-fat-diet-induced obesity and heart dysfunction are regulated by the TOR pathway in *Drosophila*. *Cell Metab* 12, 533-544 (2010).
 19. Crespo JL, Hall MN: Elucidating TOR signaling and rapamycin action: lessons from *Saccharomyces cerevisiae*. *Microbiol Mol Biol Rev* 66, 579-591, table of contents (2002).
 20. Walz G, Budde K, Manna M, Nurnberger J, Wanner C, Sommerer C, Kunzendorf U, Banas B, Horl WH, Obermuller N *et al*: Everolimus in patients with autosomal dominant polycystic kidney disease. *N Engl J Med* 363, 830-840 (2010).
 21. Rovira J, Marcelo Arellano E, Burke JT, Brault Y, Moya-Rull D, Banon-Maneus E, Ramirez-Bajo MJ, Gutierrez-Dalmau A, Revuelta I, Quintana LF *et al*: Effect of mTOR inhibitor on body weight: from an experimental rat model to human transplant patients. *Transpl Int* 21, 992-998 (2008).
 22. Yang SB, Lee HY, Young DM, Tien AC, Rowson-Baldwin A, Shu YY, Jan YN, Jan LY: Rapamycin induces glucose intolerance in mice by reducing islet mass, insulin content, and insulin sensitivity. *J Mol Med (Berl)* 90, 575-585 (2012).
 23. Deblon N, Bourgoin L, Veyrat-Durebex C, Peyrou M, Vinciguerra M, Caillon A, Maeder C, Fournier M, Montet X, Rohner-Jeanrenaud F *et al*: Chronic mTOR inhibition by rapamycin induces muscle insulin resistance despite weight loss in rats. *Br J Pharmacol* 165, 2325-2340 (2012).
 24. Zahr E, Molano RD, Pileggi A, Ichii H, San Jose S, Bocca N, An W, Gonzalez-Quintana J, Fraker C, Ricordi C *et al*: Rapamycin impairs beta-cell proliferation in vivo. *Transplant Proc* 40, 436-437 (2008).

25. Choo AY, Yoon SO, Kim SG, Roux PP, Blenis J: Rapamycin differentially inhibits S6Ks and 4E-BP1 to mediate cell-type-specific repression of mRNA translation. *Proc Natl Acad Sci U S A* 105, 17414-17419 (2008).
26. Lander ES, Linton LM, Birren B, Nusbaum C, Zody MC, Baldwin J, Devon K, Dewar K, Doyle M, FitzHugh W *et al*: Initial sequencing and analysis of the human genome. *Nature* 409, 860-921 (2001).
27. Venter JC, Adams MD, Myers EW, Li PW, Mural RJ, Sutton GG, Smith HO, Yandell M, Evans CA, Holt RA *et al*: The sequence of the human genome. *Science* 291, 1304-1351 (2001).
28. Bartel DP: MicroRNAs: genomics, biogenesis, mechanism, and function. *Cell* 116, 281-297 (2004).
29. Ul-Hussain M: Micro-RNAs (miRNAs): genomic organisation, biogenesis and mode of action. *Cell Tissue Res* 349, 405-413 (2012).
30. He L, Hannon GJ: MicroRNAs: small RNAs with a big role in gene regulation. *Nat Rev Genet* 5, 522-531 (2004).
31. Lim LP, Lau NC, Garrett-Engele P, Grimson A, Schelter JM, Castle J, Bartel DP, Linsley PS, Johnson JM: Microarray analysis shows that some microRNAs downregulate large numbers of target mRNAs. *Nature* 433, 769-773 (2005).
32. Altuvia Y, Landgraf P, Lithwick G, Elefant N, Pfeffer S, Aravin A, Brownstein MJ, Tuschl T, Margalit H: Clustering and conservation patterns of human microRNAs. *Nucleic Acids Res* 33, 2697-2706 (2005).
33. Kim VN, Han J, Siomi MC: Biogenesis of small RNAs in animals. *Nat Rev Mol Cell Biol* 10, 126-139 (2009).
34. McGregor RA, Choi MS: microRNAs in the regulation of adipogenesis and obesity. *Curr Mol Med* 11, 304-316 (2011).
35. Doghman M, El Wakil A, Cardinaud B, Thomas E, Wang J, Zhao W, Peralta-Del Valle MH, Figueiredo BC, Zambetti GP, Lalli E: Regulation of insulin-like growth factor-mammalian target of rapamycin signaling by microRNA in childhood adrenocortical tumors. *Cancer Res* 70, 4666-4675 (2010).
36. Nagaraja AK, Creighton CJ, Yu Z, Zhu H, Gunaratne PH, Reid JG, Olokpa E, Itamochi H, Ueno NT, Hawkins SM *et al*: A link between mir-100 and FRAP1/mTOR in clear cell ovarian cancer. *Mol Endocrinol* 24, 447-463 (2010).
37. Fornari F, Milazzo M, Chieco P, Negrini M, Calin GA, Grazi GL, Pollutri D, Croce CM, Bolondi L, Gramantieri L: MiR-199a-3p regulates mTOR and c-Met to

- influence the doxorubicin sensitivity of human hepatocarcinoma cells. *Cancer Res* 70, 5184-5193 (2010).
38. Jin Y, Tymen SD, Chen D, Fang ZJ, Zhao Y, Dragas D, Dai Y, Marucha PT, Zhou X: MicroRNA-99 Family Targets AKT/mTOR Signaling Pathway in Dermal Wound Healing. *PLoS One* 8, e64434 (2013).
 39. Oßwald A: Einfluss des mTOR-Signalwegs auf die differentielle microRNA-Expression während der Adipozytendifferenzierung. *Imu*; 2012.
 40. Alexander R, Lodish H, Sun L: MicroRNAs in adipogenesis and as therapeutic targets for obesity. *Expert Opin Ther Targets* 15, 623-636 (2011).
 41. Esau C, Davis S, Murray SF, Yu XX, Pandey SK, Pear M, Watts L, Booten SL, Graham M, McKay R *et al*: miR-122 regulation of lipid metabolism revealed by in vivo antisense targeting. *Cell Metab* 3, 87-98 (2006).
 42. Papadopoulos GL, Alexiou P, Maragkakis M, Reczko M, Hatzigeorgiou AG: DIANA-mirPath: Integrating human and mouse microRNAs in pathways. *Bioinformatics* 25, 1991-1993 (2009).
 43. Green H, Kehinde O: Sublines of Mouse 3t3 Cells That Accumulate Lipid. *Cell* 1, 113-116 (1974).
 44. Deutsch MJ, Schriever SC, Roscher AA, Ensenaer R: Digital image analysis approach for lipid droplet size quantitation of Oil Red O-stained cultured cells. *Anal Biochem* (2013).
 45. Brattelid T, Aarnes EK, Helgeland E, Guvaag S, Eichele H, Jonassen AK: Normalization strategy is critical for the outcome of miRNA expression analyses in the rat heart. *Physiol Genomics* 43, 604-610 (2011).
 46. Pfaffl MW: A new mathematical model for relative quantification in real-time RT-PCR. *Nucleic Acids Res* 29, e45 (2001).
 47. Lucas ES, Watkins AJ, Cox AL, Marfy-Smith SJ, Smyth N, Fleming TP: Tissue-specific selection of reference genes is required for expression studies in the mouse model of maternal protein undernutrition. *Theriogenology* 76, 558-569 (2011).
 48. Tee AR, Blenis J: mTOR, translational control and human disease. *Semin Cell Dev Biol* 16, 29-37 (2005).
 49. Heneghan HM, Miller N, Kerin MJ: Role of microRNAs in obesity and the metabolic syndrome. *Obes Rev* 11, 354-361 (2009).

50. Romao JM, Jin W, Dodson MV, Hausman GJ, Moore SS, Guan le L: MicroRNA regulation in mammalian adipogenesis. *Exp Biol Med (Maywood)* 236, 997-1004 (2011).
51. Xu J, Wong C: A computational screen for mouse signaling pathways targeted by microRNA clusters. *RNA* 14, 1276-1283 (2008).
52. Tang X, Muniappan L, Tang G, Ozcan S: Identification of glucose-regulated miRNAs from pancreatic beta cells reveals a role for miR-30d in insulin transcription. *RNA* 15, 287-293 (2009).
53. Guttilla IK, White BA: Coordinate regulation of FOXO1 by miR-27a, miR-96, and miR-182 in breast cancer cells. *J Biol Chem* 284, 23204-23216 (2009).
54. Myatt SS, Wang J, Monteiro LJ, Christian M, Ho KK, Fusi L, Dina RE, Brosens JJ, Ghaem-Maghami S, Lam EW: Definition of microRNAs that repress expression of the tumor suppressor gene FOXO1 in endometrial cancer. *Cancer Res* 70, 367-377 (2010).
55. Petrocca F, Vecchione A, Croce CM: Emerging role of miR-106b-25/miR-17-92 clusters in the control of transforming growth factor beta signaling. *Cancer Res* 68, 8191-8194 (2008).
56. Ivanovska I, Ball AS, Diaz RL, Magnus JF, Kibukawa M, Schelter JM, Kobayashi SV, Lim L, Burchard J, Jackson AL *et al*: MicroRNAs in the miR-106b family regulate p21/CDKN1A and promote cell cycle progression. *Mol Cell Biol* 28, 2167-2174 (2008).
57. Sun F, Fu H, Liu Q, Tie Y, Zhu J, Xing R, Sun Z, Zheng X: Downregulation of CCND1 and CDK6 by miR-34a induces cell cycle arrest. *FEBS Lett* 582, 1564-1568 (2008).
58. Hermeking H: The miR-34 family in cancer and apoptosis. *Cell Death Differ* 17, 193-199 (2010).
59. MacDougald OA, Lane MD: Transcriptional regulation of gene expression during adipocyte differentiation. *Annu Rev Biochem* 64, 345-373 (1995).
60. Kim JE, Chen J: regulation of peroxisome proliferator-activated receptor-gamma activity by mammalian target of rapamycin and amino acids in adipogenesis. *Diabetes* 53, 2748-2756 (2004).
61. Yeh WC, Bierer BE, McKnight SL: Rapamycin inhibits clonal expansion and adipogenic differentiation of 3T3-L1 cells. *Proc Natl Acad Sci U S A* 92, 11086-11090 (1995).

62. Witkos TM, Koscianska E, Krzyzosiak WJ: Practical Aspects of microRNA Target Prediction. *Curr Mol Med* 11, 93-109 (2011).
63. Li L, Xu J, Yang D, Tan X, Wang H: Computational approaches for microRNA studies: a review. *Mamm Genome* 21, 1-12 (2010).
64. Lewis BP, Shih IH, Jones-Rhoades MW, Bartel DP, Burge CB: Prediction of mammalian microRNA targets. *Cell* 115, 787-798 (2003).
65. Vlachos IS, Kostoulas N, Vergoulis T, Georgakilas G, Reczko M, Maragkakis M, Paraskevopoulou MD, Prionidis K, Dalamagas T, Hatzigeorgiou AG: DIANA miRPath v.2.0: investigating the combinatorial effect of microRNAs in pathways. *Nucleic Acids Res* 40, W498-504 (2012).
66. Peter ME: Targeting of mRNAs by multiple miRNAs: the next step. *Oncogene* 29, 2161-2164 (2010).
67. Heidebrecht F, Heidebrecht A, Schulz I, Behrens SE, Bader A: Improved semiquantitative Western blot technique with increased quantification range. *J Immunol Methods* 345, 40-48 (2009).
68. Taylor SC, Posch A: The design of a quantitative western blot experiment. *Biomed Res Int* 2014, 361590 (2014).
69. Laplante M, Sabatini DM: An emerging role of mTOR in lipid biosynthesis. *Curr Biol* 19, R1046-1052 (2009).
70. Xie H, Lim B, Lodish HF: MicroRNAs induced during adipogenesis that accelerate fat cell development are downregulated in obesity. *Diabetes* 58, 1050-1057 (2009).
71. Khor VK, Shen WJ, Kraemer FB: Lipid droplet metabolism. *Curr Opin Clin Nutr Metab Care* 16, 632-637 (2013).
72. Gerin I, Bommer GT, McCoin CS, Sousa KM, Krishnan V, MacDougald OA: Roles for miRNA-378/378* in adipocyte gene expression and lipogenesis. *Am J Physiol Endocrinol Metab* 299, E198-206 (2010).
73. Manning BD: Balancing Akt with S6K: implications for both metabolic diseases and tumorigenesis. *J Cell Biol* 167, 399-403 (2004).
74. Harrington LS, Findlay GM, Lamb RF: Restraining PI3K: mTOR signalling goes back to the membrane. *Trends Biochem Sci* 30, 35-42 (2005).
75. Chen C, Xiang H, Peng YL, Peng J, Jiang SW: Mature miR-183, negatively regulated by transcription factor GATA3, promotes 3T3-L1 adipogenesis through inhibition of the canonical Wnt/beta-catenin signaling pathway by targeting LRP6. *Cell Signal* 26, 1155-1165 (2014).

76. Sayed AS, Xia K, Salma U, Yang T, Peng J: Diagnosis, Prognosis and Therapeutic Role of Circulating miRNAs in Cardiovascular Diseases. *Heart Lung Circ* (2014).
77. Grange C, Collino F, Tapparo M, Camussi G: Oncogenic micro-RNAs and Renal Cell Carcinoma. *Front Oncol* 4, 49 (2014).
78. Kato M, Castro NE, Natarajan R: MicroRNAs: potential mediators and biomarkers of diabetic complications. *Free Radic Biol Med* 64, 85-94 (2013).
79. Wilfred BR, Wang WX, Nelson PT: Energizing miRNA research: a review of the role of miRNAs in lipid metabolism, with a prediction that miR-103/107 regulates human metabolic pathways. *Mol Genet Metab* 91, 209-217 (2007).

G Appendix

1. Supplementary data

Table S 1 *In silico* mTOR target prediction of rapamycin-sensitive miRNAs

MiRNAs with confirmed differential expression on day 8 of differentiation in the presence or absence of rapamycin were subjected to a stringent *in silico* target prediction. Five different prediction algorithms were used (PITA, miRanda, TargetScanS, PicTar and TargetSpy) and only miRNA-target pairs with a consensus prediction of at least 2 algorithms were considered predicted. MiRNA members of cluster 183/96/182 and family 103/107 are highlighted. 'Rapamycin effect': log₂ fold change (day 8 rapamycin treatment versus day 8 of differentiation experiments).

microRNA	rapamycin effect	Predicted mTOR pathway target genes
<i>miR-182</i>	-3.06	<i>Mapk1, Pik3r3, Rictor</i>
<i>miR-96</i>	-2.90	<i>Akt3, mTOR, Rptor, Rictor, Rps6ka6</i>
<i>miR-183</i>	-2.70	<i>Rps6ka2, Tsc1</i>
<i>miR-378</i>	-2.12	<i>Akt1, Mapk1, Cab39, Tsc1</i>
<i>miR-103/107</i>	-1.66/-2.10	<i>Eif4b, Cab39, Pik3cb, Pik3r1, Vegfa</i>
<i>miR-143</i>	-0.83	<i>Eif4b, Pik3cg, Pik3r3, Rps6ka1, Rps6ka2</i>
<i>miR-30a</i>	-0.82	<i>Prkaa2, Cab39, Pik3cd, Pik3r2, Ddit4, Rictor, Rps6kb1</i>
<i>miR-494</i>	-0.76	<i>Akt1, Akt3, Prkaa2, Ulk2, Igf1, Mapk1, Cab39, Pik3cb</i>
<i>miR-340-5p</i>	-0.72	<i>Akt3, Hif1a, Igf1, Rps6kb1</i>
<i>miR-29a</i>	0.65	<i>Akt3, Eif4e2, Igf1, Pik3cg, Pik3r1, Pik3r3, Rptor, Vegfa</i>
<i>miR-503</i>	1.01	<i>Akt3, Eif4b, Eif4e, Rictor, Vegfa</i>
<i>miR-125b-5p</i>	1.03	<i>Eif4ebp1, Rps6ka1, Vegfa</i>
<i>miR-199a-3p</i>	1.06	<i>Hif1a, mTOR, Pik3cd, Rheb, Rps6kb1</i>
<i>miR-214</i>	1.06	<i>Akt2, Akt3, Ulk1, Eif4b, Igf1, Cab39, Pik3cb, Pik3r3, Rictor, Rps6ka1, Vegfa</i>
<i>miR-222</i>	1.61	<i>Prkaa2, Pik3r1, Ddit4, Rps6kb1, Tsc2</i>

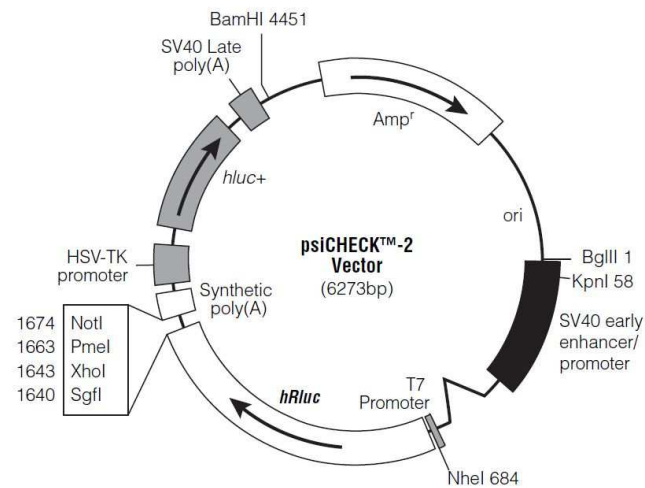


Figure S 1: Plasmid map of psiCHECK™-2 Vector

3'UTRs of predicted target genes were cloned into *NotI* and *AsiI* restriction sites. (From Technical Bulletin of siCHECK™ Vectors, Promega, Wisconsin, USA).

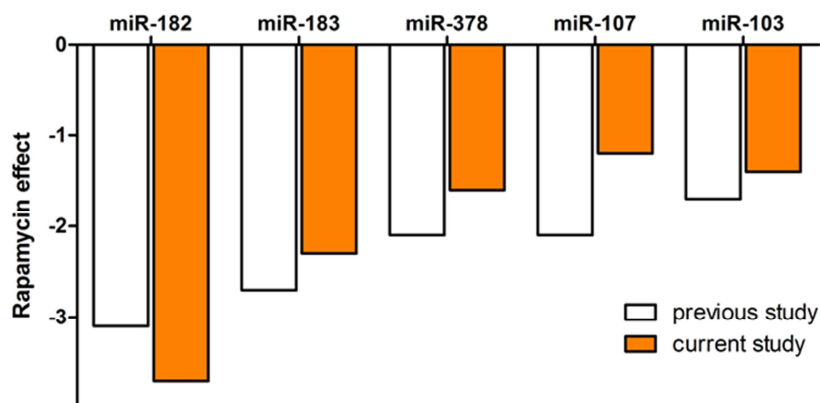


Figure S 2: Rapamycin-dependent miRNA expression changes during 3T3-L1 adipogenic differentiation

'Rapamycin effect': $\log_2(\bar{x}_{\text{fold change}_{\text{day 8 with rapamycin}}} - \bar{x}_{\text{fold change}_{\text{day 8}}})$. Previous study: RNA of 2 independent experiments was isolated at day 0 and day 8 of differentiation with and without rapamycin treatment and quantified using miRNA microarray. Current study: RNA of 2 independent experiments was isolated at day 0 and day 6 of differentiation with and without rapamycin treatment and quantified using rt-PCR.

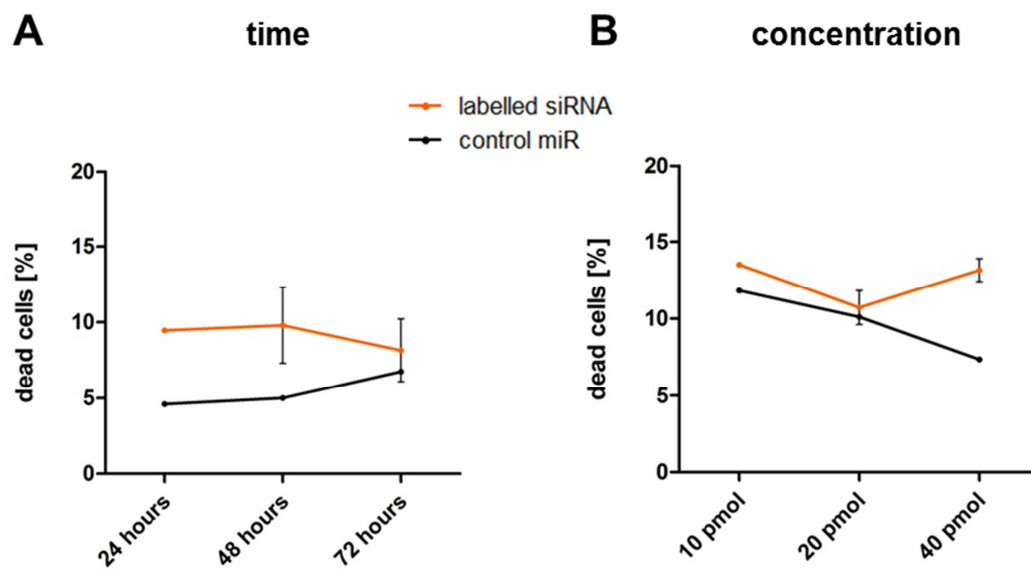


Figure S 3: Cell viability in transfection experiments

Graph shown percentage of dead cells measured *via* flow cytometry. 3T3-L1 pre-adipocytes were transfected with a labelled siRNA or an un-labelled control miRNA and stained with 7-AAD. (A) Cells were transfected with 20 pmol labelled siRNA/control miRNA and harvested at different time points *post* transfection. (B) Cells were transfected with different concentrations of labelled siRNA and harvested 24 hours *post* transfection. Mean values \pm S.E.M. of 2 independent experiments. 10,000 cells were analyzed for each treatment group.

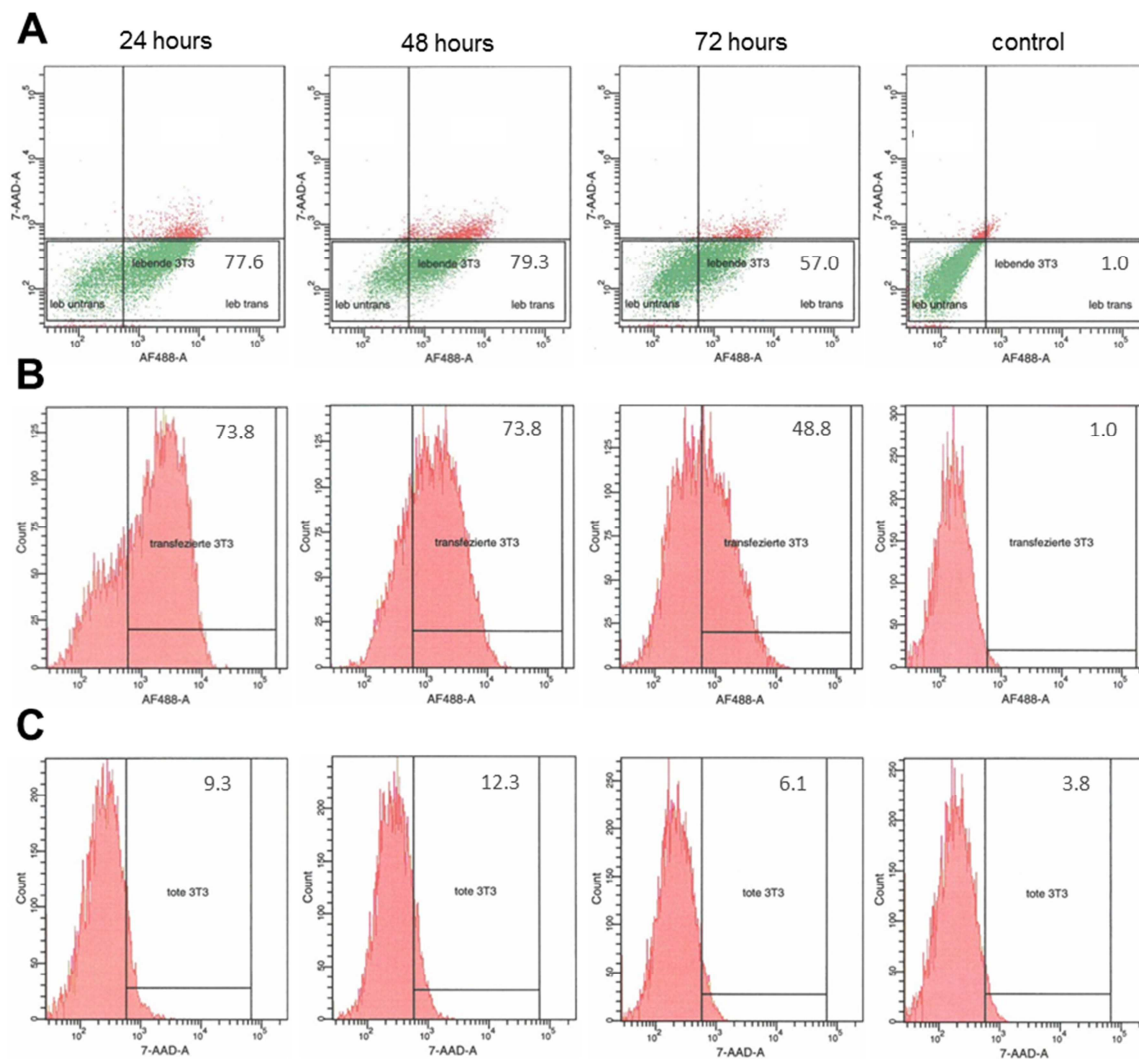


Figure S 4: Flow cytometry of transfected 3T3-L1 pre-adipocytes 24, 48 and 72 hours *post* transfection

(A) Representative flow cytometry plots show intracellular AF-488 versus 7-AAD staining. Representative histograms indicate analyzed events versus (B) AF-488 or (C) 7-AAD intensity in 3T3-L1 cells transfected with an AF-488-labelled siRNA 24, 48 and 72 hours *post* transfection. Cells were transfected with 20 pmol siRNA per well. Control cells were transfected with an unlabelled control miRNA. Numbers in plots and histograms stand for the percentage of cells in the gated population.

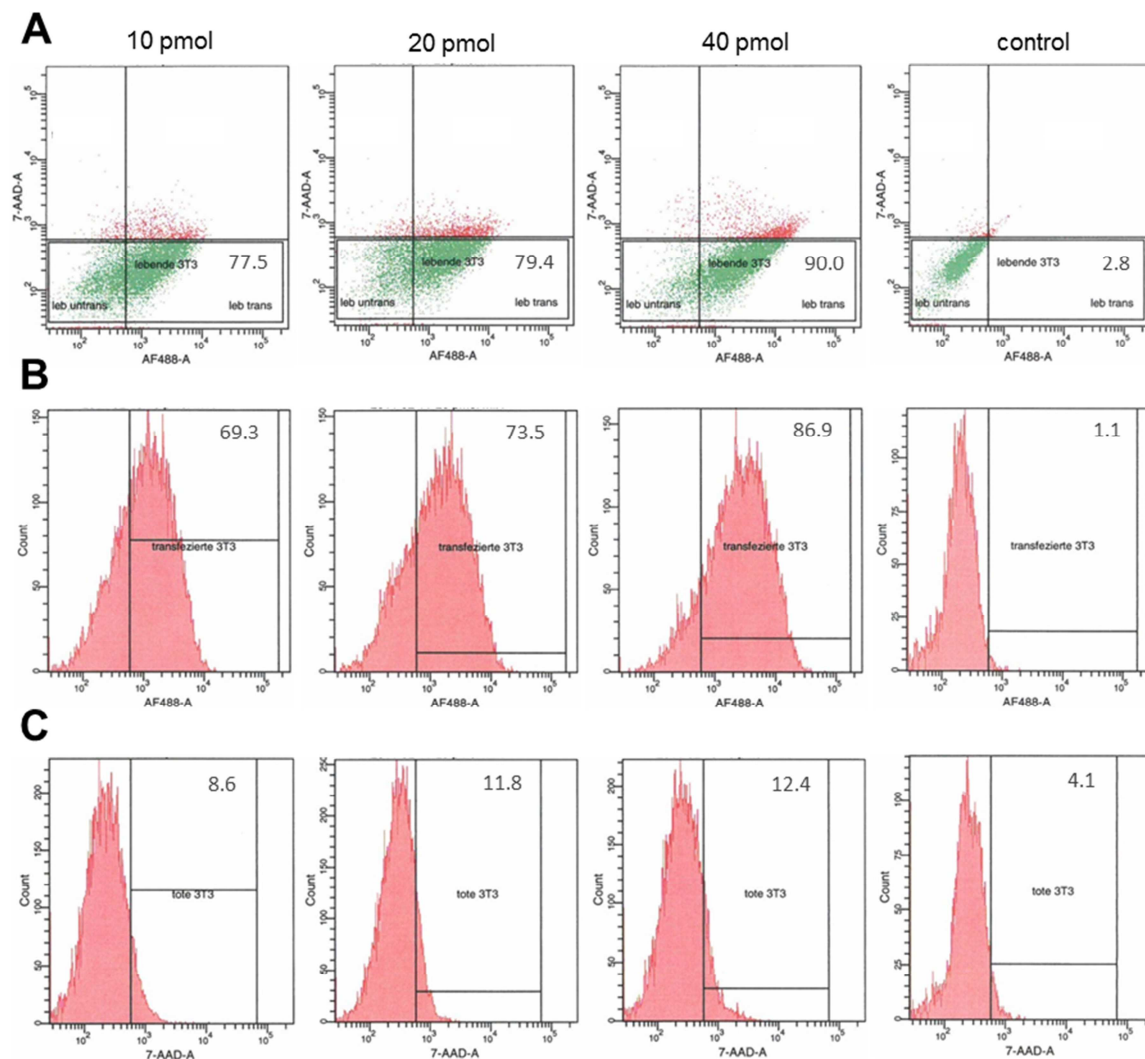


Figure S 5: Flow cytometry of 3T3-L1 pre-adipocytes transfected with 10, 20 and 40 pmol AF-488-labelled siRNA

(A) Representative flow cytometry plots show intracellular AF-488 versus 7-AAD staining. Representative histograms indicate analyzed events versus (B) AF-488 or (C) 7-AAD intensity in 3T3-L1 cells transfected with 10, 20 and 40 pmol AF-488-labelled siRNA per well. Cells were harvested 24 hours *post* transfection. Control cells were transfected with an unlabelled control miRNA. Numbers in plots and histograms indicate the percentage of cells in the gated population.

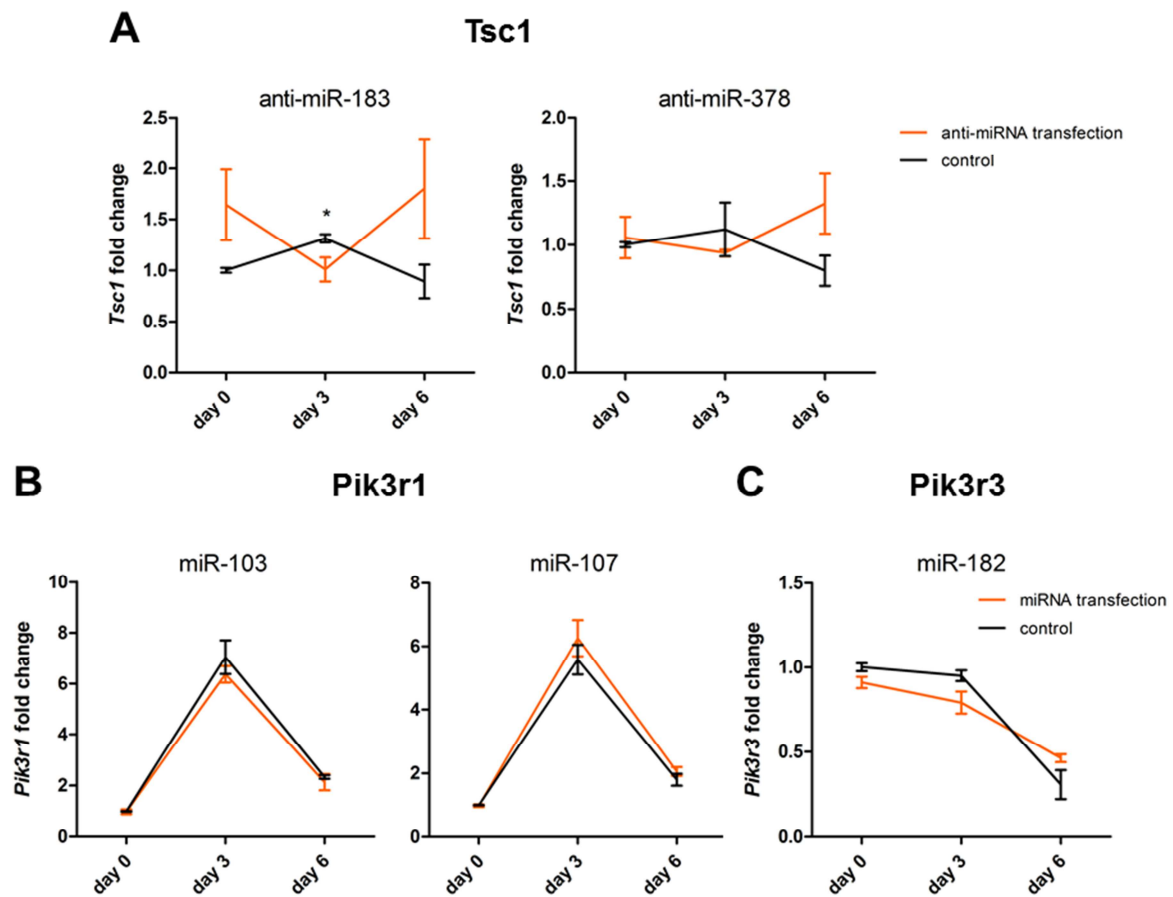


Figure S 6: MiRNA effects on target transcript levels during 3T3-L1 adipogenic differentiation

Transcript levels were quantified using rt-PCR in 3T3-L1 cells transfected with different Pre-miRTM miRNA Precursors and subsequently differentiated. (A) *Tsc1* (B) *Pik3r1* and (C) *Pik3r3* transcript levels are shown. Gene expression was normalized to the respective expression levels in control cells at day 0 of differentiation. Mean values \pm S.E.M. of 2 independent experiments each performed in technical triplicates.

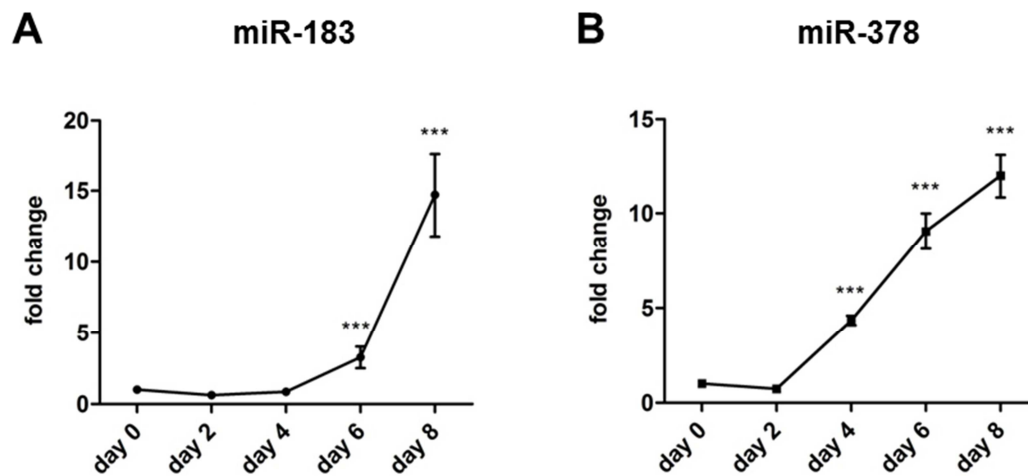


Figure S 7: Increase in miR-183 and -378 expression during the late phase of 3T3-L1 adipogenic differentiation

Rt-PCR quantification of miRNA levels over 8 days of differentiation. Expression changes of (A) miR-183 and (B) miR-378 levels, normalized to day 0 expression are shown. Mean values \pm S.E.M of 2 independent experiments, each performed in technical triplicates. Asterisks show significant regulation as compared to day 0. *** $P \leq 0.001$.

2. List of abbreviations

7-AAD	7-amino-actinomycin D
Actb	beta actin
Akt	v-akt murine thymoma viral oncogene
(c)AMP	(cyclic) adenosine monophosphate
Ampk	AMP-activated protein kinase (gene name Prkaa2)
bp	base pair
BMI	Body Mass Index
BSA	bovine serum albumin
Cab39	calcium binding protein39
C/ebp	CCAAT/enhancer binding protein
Ddit	DNA-damage-inducible transcript
Dlk1	delta-like 1 homolog
DMEM	Dulbecco's Modified Eagle Medium
DMSO	dimethyl sulfoxide
DNA	deoxy ribonucleic acid
dNTP	deoxy nucleoside triphosphate
DTT	dithiothreitol
4Ebp1	eukaryotic translation initiation factor 4E binding protein 1
EDTA	ethylenediaminetetraacetic acid
eIF4a/b/e/g	eukaryotic translation initiation factor 4A/B/E/G
eIF4ebp1	eukaryotic translation initiation factor 4E binding protein 1
Exp-5	Exportin-5
FACS	Fluorescence-activated cell sorting
FBS	Fetal Bovine Serum
Fkbp12	FK506-binding protein 12
GβI	G-protein beta-subunit-like
Hif1	hypoxia inducible factor 1
Hprt	hypoxanthine guanine phosphoribosyl transferase
IBMX	3-Isobutyl-1-methylxanthine
Igf	insulin-like growth factor
KEGG	Kyoto Encyclopedia of Genes and Genomes
LB-Amp ¹⁰⁰	Luria Bertani medium containing 100 µg/ml ampicillin
LDA	Low density array
M	Molar

Mapk	mitogen-activated protein kinase
miR/miRNA	microRNA
mTOR	mammalian target of rapamycin
mTORC1/2	mammalian target of rapamycin complex 1/2
PBS	Phosphate buffered saline
<i>Pfu</i>	<i>Pyrococcus furiosus</i>
Pho	phosphate
Pik3r1	phosphatidylinositol 3-kinase regulatory subunit 1 (alpha)
Pik3r3	phosphatidylinositol 3-kinase regulatory subunit 3 (gamma)
Ppar γ	Peroxisome proliferator-activated receptor gamma
Ppib	peptidylprolyl isomerase b (cyclophilin B)
Pref-1	pre-adipocyte factor-1
pre-miRNA	precursor microRNA
pri-miRNA	primary microRNA
Prkaa2	AMP-activated protein kinase alpha 2 catalytic subunit
Rheb	Ras homolog enriched in brain
Rictor	Rptor independent companion of mTOR complex 2
RISC	RNA-induced silencing complex
Rn18s	18S ribosomal RNA
Rps6ka	p90 ribosomal protein S6 kinase
Rps6kb	p70 ribosomal protein S6 kinase
Rptor	regulatory associated protein of mTOR complex 1
Rsk	p90 ribosomal protein S6 kinase
RT	Reverse Transcription
rt-PCR	real-time PCR
S6k1	p70 ribosomal protein S6 kinase 1
SDS software	Sequence Detection Systems software
SDS	sodium dodecyl sulfate
TAE	Tris-acetate-EDTA
TRIS	Tris (hydroxymethyl)-aminomethan
Tsc1/2	tuberous sclerosis protein 1/2
Ube2d2	ubiquitin-conjugating enzyme E2D2A
Ulk	Unc-51like kinase
UTR	untranslated region
Vegfa	vascular endothelial growth factor A

3. Curriculum vitae and publications

Education

- 2010-2015 Ludwig-Maximilians Universität München
Degree: Dr. rer. nat. (expected)
- 2004-2009 Technische Universität München, Weihenstephan
Degree: Diploma (Dipl. biol.)
- 1995-2004 Deutschherren-Gymnasium Aichach
Degree: Abitur

Experience

- 2013-present Klinikum der Ludwig-Maximilians Universität München
BMBF project »Towards newborn screening for primary immunodeficiencies«

Skills

LMUexcellent: Program of the Center for Leadership and People Management:
»Exzellent führen. Führend forschen.«

GWT Gesellschaft für wissenschaftlichen Tierschutz: Versuchstierkundlicher Kurs
FELASA Kategorie C

Graduate Center of LMU workshops: Presentation skills, Communication and Teams,
Project Management, Scientific Writing, Writing Proposals

Publications

Kaeuferle T., Osswald A., Fleischmann K.K., Pagel P., v. Frowein J., Krauss-Etschmann S., Roscher A.A., *Identification of microRNAs involved in mTOR nutrient signaling during adipogenesis* in JABB 2394-1081, Vol.: 2, Issue.: 2

Kaeuferle T., Bartel S., Dehmel S., Krauss-Etschmann S., *MicroRNA methodology: advances in microRNA technologies* in Methods Mol Biol. 1169: 121-30, 2014

4. Acknowledgements

Without the support, encouragement and guidance of the following people, this dissertation would not have been completed.

Firstly, I would like to acknowledge the help and support of my supervisors Prof. Dr. Adelbert Roscher and PD Dr. Susanne Krauss-Etschmann on this research program. Thank you for giving me the scientific freedom to follow my own ideas. I am also very thankful to Prof. Klaus Förstemann for being my “Fachvertreter”.

Further, I would like to thank all the present and past members of Krauss-Etschmann and Oncology Research Group for all the enlightening discussions we had in lab meetings. Thanks Gaby Heilig and Conny Dalibor for your commitment in endless numbers of PCRs and RNA isolations. Specifically, I would like to thank Manish Aneja, Inge Kepert and Katrin Fleischmann for being wonderful lab colleagues. Thanks Manish for your insight and discussions on several research topics and lab instrumentation as well as your helpful advice for every life situation. Thanks Inge for cheering me up in times of frustration and thanks Katrin for your grand help with the publication.

I want to thank my family for their love and support, but also their patience during times when I was occupied with work. I want to thank with all my heart my brother Uli and his wife Mony, they always helped me to find inner peace and the will power to go on in times of frustration.

But life is more than science. Therefore special thanks goes to all members of the “Held”-family for supporting me by taking over all work and training of my horse in times of ‘deadlines’ and work overload. Sincere thanks to Heiner, who created an excellent, funny, exciting and thrilling world full of sporty challenges for me. Thanks Renate for your flexibility and numerous spontaneous dressage lessons around lab times, without those international competitions would not have been possible. You all provided a perfect counterbalance to academic life.

Lastly I would like to acknowledge my funding and graduate program “Graduiertenkolleg 1202” for their financial support and the opportunities for further trainings and skill enhancement. Thanks to all GraKo members for crazy evenings at Corleone pub and amazing trips to retreats and workshops. I will miss you all.